MAPPING OF LINEAR GEOLOGIC STRUCTURES AT MOUNTAIN TOP UNIVERSITY'S PERMANENT SITE, MAKOGI-OBA, OGUN STATE, NIGERIA USING AEROMAGNETIC AND 2D ELECTRICAL RESISTIVITY TOMOGRAPHY DATA

By

JOSHUA Daniel Toluwase

17010401001

A PROJECT SUBMITTED TO THE DEPARTMENT OF GEOSCIENCES, COLLEGE OF BASIC AND APPLIED SCIENCES, MOUNTAIN TOP UNIVERSITY, PRAYER CITY, OGUN STATE, NIGERIA

IN PARTIAL FULFILMENT OF THE REQUIREMENTS FOR THE AWARD OF BACHELOR OF SCIENCE (B. Sc.) DEGREE IN GEOPHYSICS

SEPTEMBER, 2021

DECLARATION

I hereby declare that this project has been written by me and is a record of my own research work. It has not been presented in any previous application for a higher degree of this or any other University. All citations and sources of information are clearly acknowledged by means of reference.

_____

JOSHUA, Daniel Toluwase

_____

Date

CERTIFICATION

This is to certify that the content of this project entitled **"Mapping of Linear Geologic Structures at Mountain Top University's Permanent Site, Makogi-Oba, Ogun State, Nigeria using Aeromagnetic and 2D Electrical Resistivity Tomography Data"** was completed and submitted by **JOSHUA, Daniel Toluwase** with matriculation number **17010401001,** in partial fulfillment of the requirements for the award of **BACHELOR OF SCIENCE (B.Sc.) DEGREE IN GEOPHYSICS**. The original research work was carried out by him under my supervision and is hereby accepted.

PROFESSOR ELIJAH A. AYOLABI _____

Supervisor *(Signature and Date)*

DR. O. B. BALOGUN _____

Supervisor *(Signature and Date)*

DR. O. B. BALOGUN _____

Head of Department *(Signature and Date)*

DEDICATION

This project is dedicated to “THE ALMIGHTY GOD” for the enabling strength HE bestowed on me to complete this work. Secondly, to my wonderful parents Mr. and Mrs. Ajayi Joshua who supported me both financially and morally.

ACKNOWLEDGEMENTS

I am most grateful to God Almighty, the sole provider of wisdom, knowledge and understanding, for his protection throughout the period of the programme.

Also, I appreciate the Chancellor, Dr. D. K. Olukoya for his financial and spiritual support during my period of study. I sincerely appreciate the efforts of my supervisors, Professor E. A. Ayolabi and Dr. O. B. Balogun for their tireless efforts in supervising this research project. Their mentorship, endurance, patience and constructive criticism and corrections saw me through the various phases of this project work.

I appreciate my parents, Mr. and Mrs. Ajayi Joshua, for their unquantifiable love and financial support during the whole period of my study at Mountain Top University. I also want to appreciate every member of staff who has in one way or the other contributed to my success in Mountain Top University. These include the entire members of staff of the Department of Geosciences and the following people: Mrs. Bakare (VC's office), Mrs. A. E. Soyinka, Pastor Olumide Adesina, Pastor Olumide Tanimowo and Mr. Osayande Osaghae.

In addition, I will like to appreciate my friends, brothers and sisters who have been with me from the start Lateef Abosede, Adebami Teminijesu, Oluwafemi Moyo Faith, Fadumo Adebowale, Fasanmade James, Ibeauchi Innocent, Adeyemi Tijesunimi, Olaitan Philip, Oladapo Feranmi and Atoyebi Ayomide.

Finally, I want to appreciate my dearest Joshua Victor, Joshua Tosin, Joshua Testimony, Adeyemo Toluwani, Uzochukwu Shalom and Babatunde Emmanuel.

TABLE OF CONTENTS

CHAPTER TWO

BASIC THEORY OF MAGNETIC METHOD

LIST OF FIGURES

ABSTRACT

Aeromagnetic and 2D Electrical Resistivity Tomography (ERT) data have been processed, integrated and interpreted for the purpose of mapping linear geologic structures at Mountain Top University's permanent site in Makogi-Oba, Ibafo area of Ogun State which is currently being considered for development. The study was aimed at mapping linear geologic structures whose occurrences are to be given proper consideration in order to optimise land usage in the physical planning of the study area for development.

The total magnetic field intensity (TMI) data were reduced to the magnetic equator to remove asymmetries associated with low magnetic latitude anomalies and was subsequently separated into its regional and residual field constituents. The residual field was enhanced using various techniques which included the Total Horizontal Derivative (THD), Standard Euler Deconvoluion and Tilt Derivative (TDR). Four 1110 m long 2D ERT profiles, probing a depth of about 220 m, were also acquired in the study area using the dipole-dipole array. The data were inverted using the "EarthImager^{TM}" software.

The TMI map was observed to be dominated by elongated to linear magnetic anomalies trending mostly in the approximate N – S direction. Though having a low magnetic relief of about 2.6 nT, the study area reflected four magnetic field intensity zones which were characteristically distinct with magnetic intensity decreasing from West to East. The pattern of the decreasing magnetic intensities eastwards seemed to be suggestive of a step-faulting phenomenon with depth to the faulted blocks decreasing eastwards. The residual field map comprised of both elongated and spherical magnetic anomalies, some with relatively high magnetic intensities while others had relative low magnetic intensities. An intersection of magnetic lows in the eastern part of the study area was identified and interpreted to suggest that the study area is a shear zone. The lineaments delineated by the THD comprised of long, intermediate and short lineaments. From the THD map, the western and southern parts consist mostly of long and intermediate lineaments while the northeastern part was found to be dominated by short lineaments. The Euler Deconvolution mostly resolved long lineaments and their appendages but resolved less of isolated short lineaments. The integrated result of the THD and Euler deconvolution derived lineaments appreared to agree in a good part of the study area while in some parts it can be best described as complementary. From

the Euler Deconvolution solutions, depth estimates to the linear geologic structures rarely exceeded 200 m except in the central southern and central northern parts. Tilt derivative solutions presented depths to some delineated semi-regional to regional scaled structures as ranging between 102.94 m and 286.76 m. The 2D ERT inverted section imaged three to four geoelectric layers which were interpreted as interclation of sand and clay. The immediate topsoil was found to be clayey and its thickness approached 8 m in some regions. Some structure suspected to be faults, coincident with the delineated magnetic lineaments, were imaged on the 2D ERT sections.

The study area was found to be a shear zone having lots of linear geologic structures within it. The northwestern part of the study area appeared to be the least affected by the presence of linear geologic structures and may require less stabilisation for construction. The immediate topsoil being clayey, geotechnical competence tests may be required for the subgrade soil. To optimise the groundwater resources in the area, the linear geologic structures should be intersected at the northern region where they dip towards.

CHAPTER ONE

INTRODUCTION

1.1 Preamble

Obtaining data about the subsurface either from the extrapolation of surface geological information or from direct measurement of physical properties of rocks and earth materials by geophysical methods is still the most potent fundamental means of deriving knowledge about structural disposition of an area (Reynolds, 2011; Parsekian *et al.,* 2015).

Various geophysical methods are often applied to solve specific geological problems especially when the nature of the study requires rapidity and less disturbance of the subsurface (Lowe and Zaccheo, 1991; O'Neil, 2001; Holden *et al.,* 2002; Rana, 2019). Geological problems often requiring geophysical solutions include exploration and mining studies, groundwater/hydrological studies, environmental and nuclear studies, and engineering site investigations and developmental planning (Fairbridge *et al.,* 1998; National Research Council, 2004; Gore and Davies, 2013).

Engineering site investigations and developmental planning is an aspect of geophysics, which though have been practiced for decades, is just gaining recognition and patronage in the developing economies of the world (Ribes and Finholt, 2009; Curtis and Low, 2016). It is gradually becoming obvious that modern civil engineering practices need information about the conditions of the subsurface (geologic information) as much as it needs accurate structural detailing which in time past has usually been their singular focus in order to maximise land resources (Walters, 2008; Griffiths and King, 2013; Dearman, 2013).

Some of the most effective geophysical methods for engineering site investigations and developmental planning include seismic refraction method (Cardarelli *et al.,* 2010; Adamo *et al.,*

2021), electrical methods (Oyedele and Olorede, 2010; Cardarelli *et al.*, 2010; Hossain *et al*., 2010), magnetic methods (Adagunodo *et al.*, 2015; Balogun, 2019; Oyeniyi *et al.*, 2016) and gravity method (McDowell *et al.*, 2002; Davis *et al.*, 2008) e.t.c.

Magnetic and electrical (electrical resistivity) methods remain two of the most patronised methods in engineering site investigation and developmental planning because of its affordable instrumentation and ease of use (Bogoslovsky and Ogilvy, 1997; Robinson *et al.*, 2008; Cardarelli *et al.*, 2010). Magnetic survey data often depict differences in the earth's magnetic field caused by the magnetic characteristics of the underlying rocks (e.g. magnetic susceptibilities). Magnetic susceptibility is lowest in sedimentary rocks, whereas it is highest in metamorphic and acidic igneous rocks, intermediate and basic igneous rocks (Telford *et al.*, 1990; Kearey *et al*., 2002). Magnetic survey can be land borne (ground magnetic survey), ship borne (ocean magnetic survey) or air borne (aeromagnetic survey) (Kearey *et al.*, 2002; Telford *et al.*, 1990; Reynolds, 1997).

Geologic zones of structural weaknesses (fracture and shear zones) can be delineated from aeromagnetic survey data (Udensi and Osazuwa, 2004; Balogun, 2019). Such zones of weakness have been known to be prospective hosts for a range of minerals. They are also indicators for exploring epigenetic, stress-related mineralization in rocks (Paterson and Reeves, 1985). They could as well serve as potential productive regions for ground water abstraction (Oni *et al.*, 2020), however, their occurrence in large numbers and diverse orientations may render a place not suitable for construction purposes (Isaksson *et al*, 2017; Momoh *et al.*, 2008).

Electrical resistivity is a useful and reliable technique widely used in engineering site investigations to locate faults and fissures, sub-surface cavities, delineate permafrost and thaw zones, locate mineshafts and evaluate relative competence of soil layers in-situ (Griffiths and King, 2013).

One of the most significant pieces of information needed for planning in pre-construction site study, where geophysics has grown into a reliable, fast, cost-effective, and non-invasive tool, is the knowledge of the orientation, distribution, and deep extent of linear geologic features which include fractures and rock contacts (Isaksson *et al*, 2017). In most situations where pre-construction site research studies were deemed superfluous, avoidable structural flaws were discovered, and a large amount of money would have been squandered at this point (Mattsson and Wahlgren, 2010).

As a result, major construction companies have begin to spend in pre-construction studies that include geophysical mapping of linear geologic features, many of which could be harmful to engineering constructions. The benefit of such pre-construction mapping is that resources are conserved, land is effectively utilized, engineering buildings are guaranteed to be durable, and human lives are not put at risk.

In line with this evolving good practice of pre-construction site investigation consisting of various geophysical methods for mapping linear geologic structures that could pose threats to civil engineering structures, Mountain Top University's permanent site at Makogi-Oba, Ibafo area of Ogun State was investigated for potential linear geologic structures that could be inimical to engineering structures using the aeromagnetic data.

1.2 Statement of the Problem

Mountain Top University’s permanent site is currently being considered for infrastructural development. Infrastructural development, which includes physical planning and construction, had over the years evolved to require a comprehensive knowledge of the structural disposition of the subsurface such that before it can be considered suitable for construction, the subsurface must be

free of geologic structures (such as faults and joints) that could be inimical to engineering structures.

While Civil engineers have been able to come up with standard benchmarks for structural designs, it is still required that they are furnished with information about the geologic structures within the subsurface so that they can be guided in their choice of suitable sites for construction. In order to guide the engineers that will undertake projects at Mountain Top University's permanent site so that their choice of construction sites will be suitable, and to ensure proper mitigation plans in areas where inimical geologic structures are unavoidable, magnetic method of geophysical prospecting was employed to delineate risk zones so that they can either be avoided or plans can be made to lessen the risk they may pose.

1.3 Study Area

1.3.1 Description of Study Area

The study area is the Mountain Top University's permanent site in Makogi-Oba community, off Lagos-Ibadan Expressway, Ibafo area, Ogun State, Nigeria. With reference to the WGS'84 datum, the area falls between Latitudes 06.7365^{o} N and 06.7513^{o} N; and Longitudes 03.3766^{o} E and 03.3911^{o} E. Expressed in Universal Transverse Mercator (UTM) coordinates with reference to WGS'84 datum, the area is delimited by Latitudes 744640 and 746280 mN; and Longitudes 541620 and 543225 mE. Figure 1.1 is the location map of the study area.

1.3.2 Relief, Climate and Vegetation

1.3.2.1 Relief

From the elevation map of the study area (Figure 1.2), the study area can best be described as comprising significantly of low-lying areas flanked to the east, southwest and northwest by elevated portions. Having the least and maximum elevations as 6.2 and 22.7 m respectively, the relief is computed as 16.5 m. The river draining the area is the seasonal River Ipamorisha which

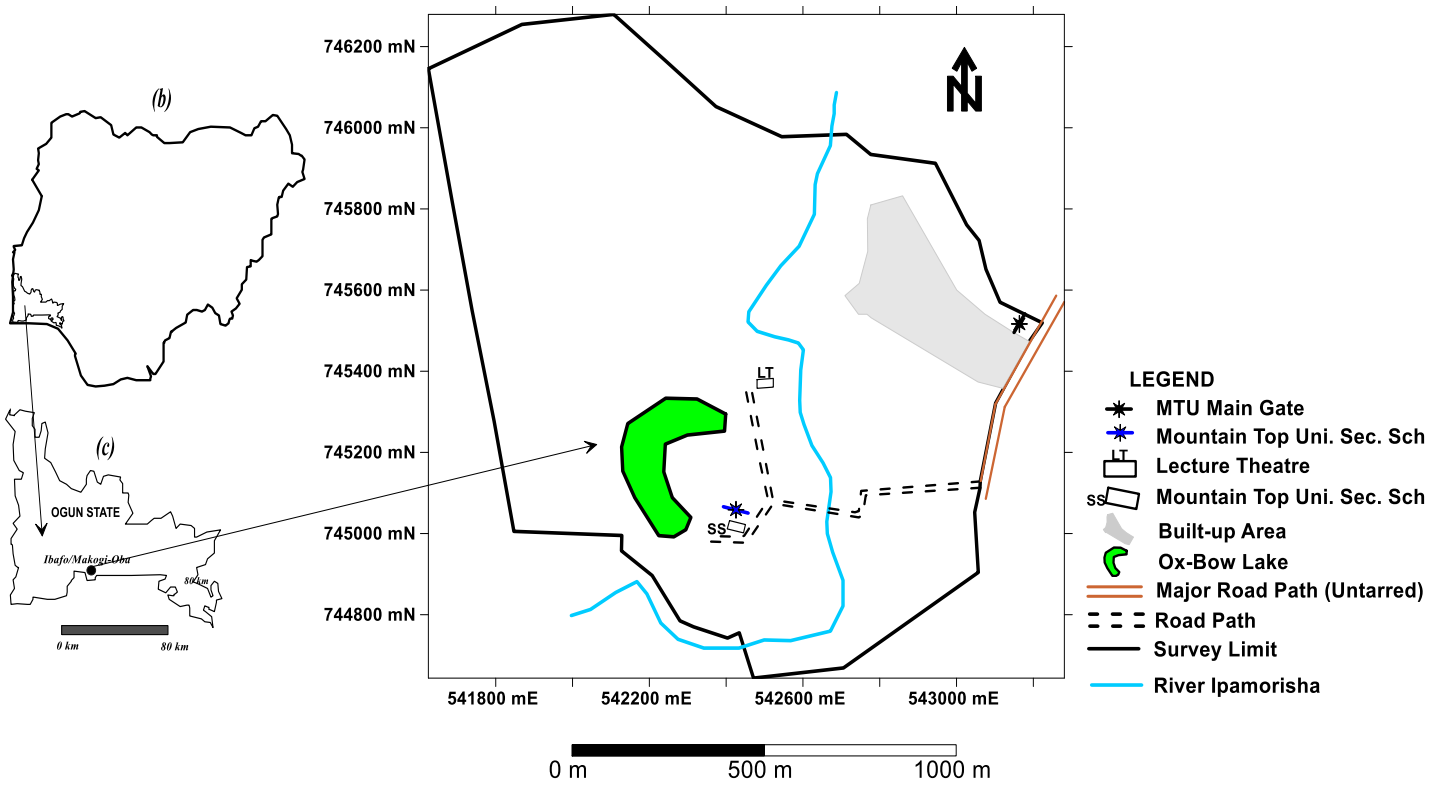

Figure 1.1: Location Map of the Study Area (*Digitised after Google Maps, 2021*)

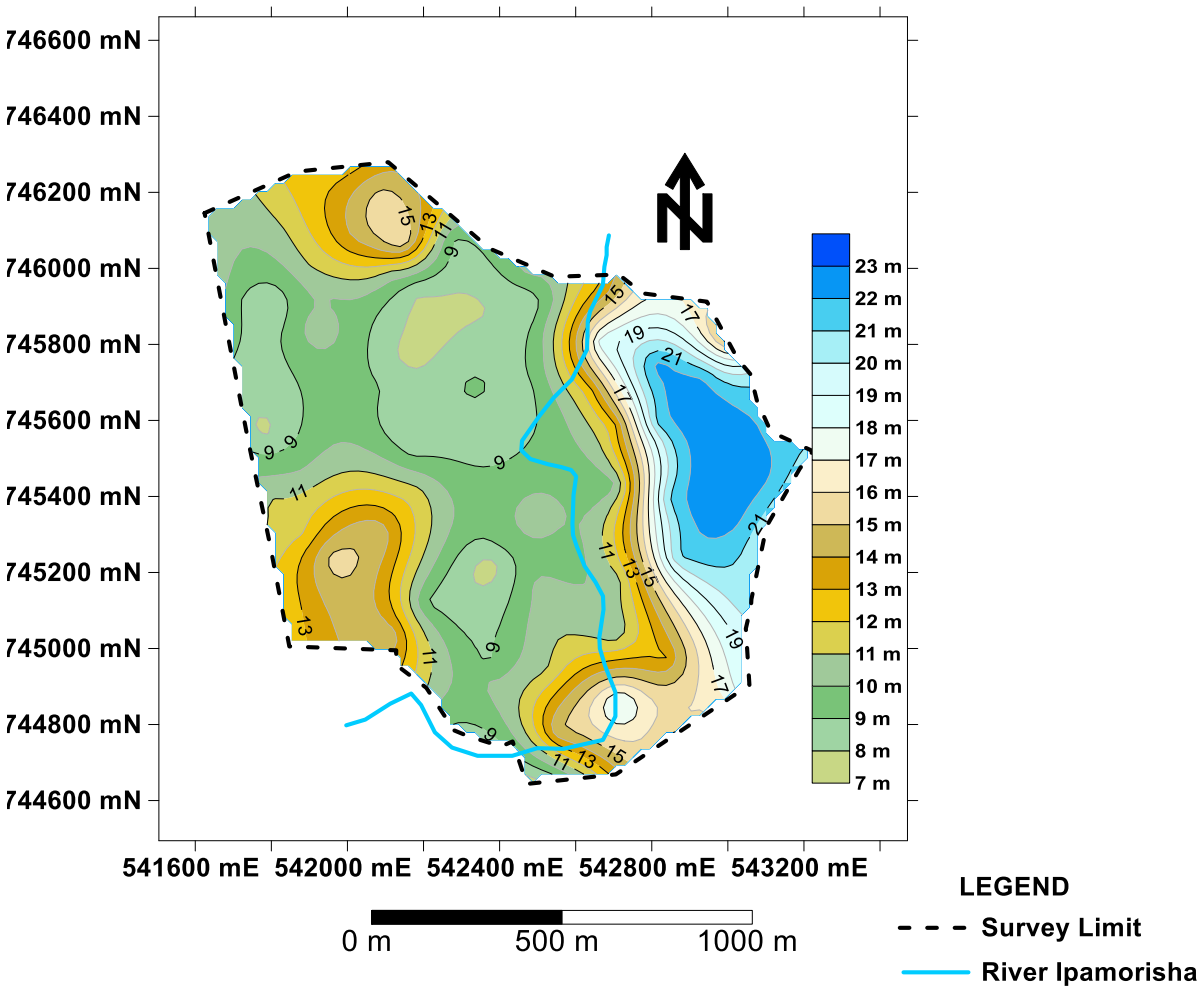

Figure 1.2: Elevation Map of the Study Area (*Obtained from SRTM (USGS, 2006)*)

is a tributary of River Ogun whose channel is located 5 km due east. The study area is within the floodplains of the Ogun river.

1.3.2.2 Climate

The region experiences two climatic seasons which are the dry and wet seasons. The dry season spans from November to March, and the wet season from April to October (Adeleke and Leong, 1978). Available rainfall data shows that rain falls throughout the whole year but a noticeable sharp decrease is usually observed from November to March. Average rainfall is 1693 mm per year while average temperature is 27.0º C (Climate-data.org).

1.3.2.3 Vegetation

Ibafo (Makogi-Oba) is a wetland region. The vegetation of Ibafo is very similar to the vegetation observed generally in Lagos State, Nigeria. Just as in Lagos State, the vegetation can be classified as a typical swamp forest consisting of freshwater regions/freshwater swamp forest (Lagos State Government, 2015). In the flood plain regions, only grasses tolerant of heavy water are present.

1.3.3 Geology of the Study Area

1.3.3.1 Regional Geology of the Study Area

The study area is located in the western part of the Nigerian sector of Dahomey Basin. The basin has been said to have been formed as a result of the Mesozoic splitting of the South America and Africa plates (de Klasz and Du Chene, 1978). Non-fossiliferous folded rocks of unknown thickness but of pre-Albian (early Cretaceous) age, are the oldest deposits in the basin. Pleistocene through Recent strata are the youngest deposits. Omatsola and Adegoke (1981) ascribed the Cretaceous strata to the Abeokuta Group and grouped them into three formations: the Ise Formation (oldest), the Afowo Formation, and the Araromi Formation (youngest). The Araromi Formation is overlain by the Ewekoro Formation, which is also overlain by the Oshosun Formation whose continuity is limited laterally.

1.3.3.2 Local Geology of the Study Area

The study area lies within the Recent Alluvium region of the Nigerian sector of the Dahomey basin, southwestern Nigeria (Figure 1.3). As observed from the geologic map, a northeast-southwest trending fault has been mapped to cut through the study area by the Nigerian Geological Survey Agency (NGSA) from remotely sensed satellite imagery (Figure 1.3).

1.4 Aim and Objectives of the Study

This study is aimed at delineating geologic lineaments present at Mountain Top University's permanent site from integrated aeromagnetic and 2D electrical resistivity tomography (ERT) data in order to make the information available for consideration during site development.

The following are the specific objectives of the research

(i) to reduce the aeromagnetic data to the magnetic equator and separate the regional and residual magnetic fields;

(ii) to perform basic structural enhancement operations which include Total Horizontal Derivative (THD), Euler Deconvolution and Tilt Derivative (TDR) operations on the residual TMI field data;

(iii) to identify the magnetic lineaments delineated within the study area;

(iv) to acquire 2D ERT data in parts of the region covered by the aeromagnetic data and invert the data;

(v) to integrate the magnetic lineaments obtained from the processed aeromagnetic data and the inverted image of the 2D ERT and check for consistency in the results of both methods; and

(vi) to present the lineament map of magnetic lineaments found within the study area.

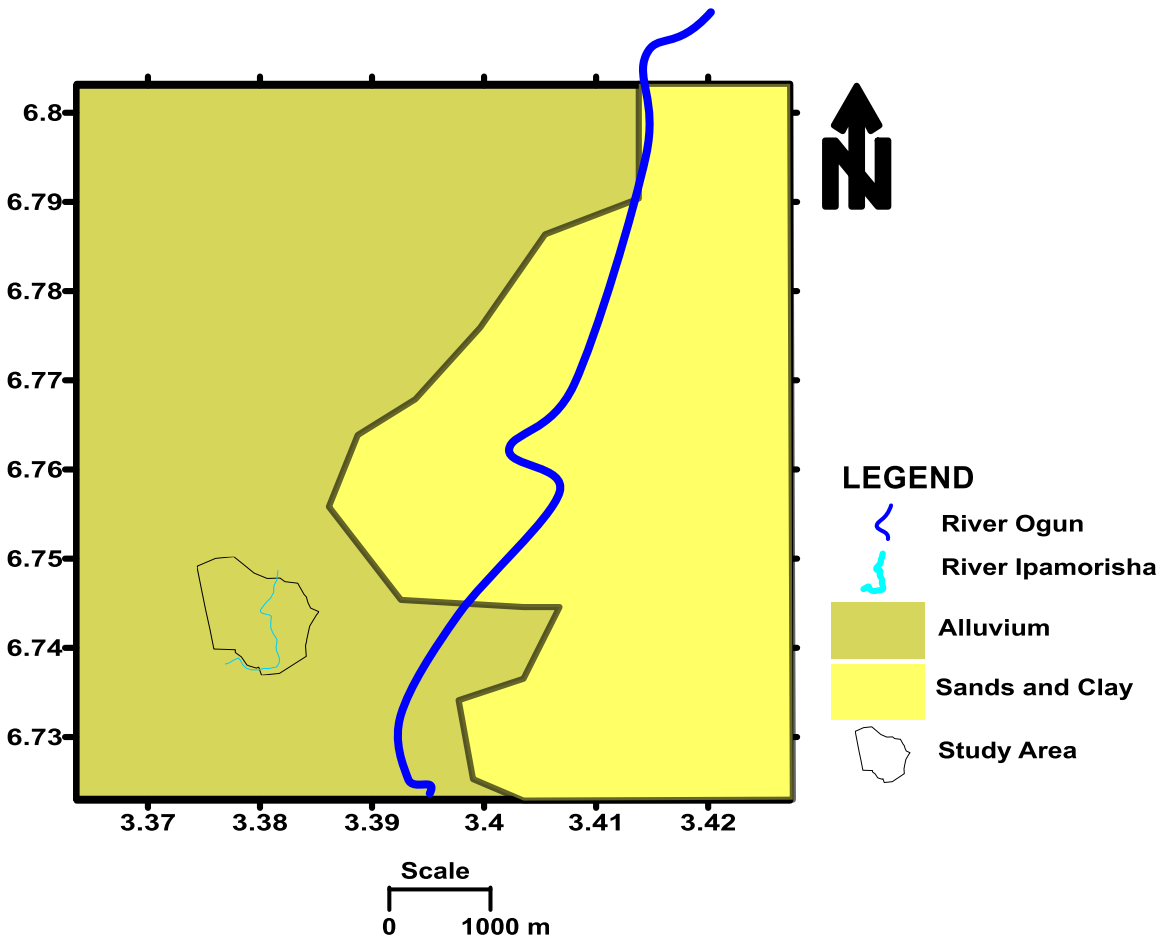

Figure 1.3: Geologic Map of the Study Area (Digitized after Nigerian Geological Survey Agency, 2006).

1.5 Literature Review

Enhancement of magnetic data by various mathematical operations (known as enhancement technique) has proved to become reliable as a means of rapidly checking the subsurface for geologic structural discontinuity (Oyeniyi *et al.,* 2014; Balogun, 2019; Oni *et al.,* 2020). This practice has continued to gain more popularity and patronage because it is effective and reliable, easily applicable to vast potential field data and the mathematical procedure are not very complex (Blakely, 1996; Ferreira *et al.,* 2013).

The enhancement methods commonly applied include the Total Horizontal Derivative (THD), Second Vertical Derivative (SVD), Analytical Signal (AS), Tilt Derivative (TDR), Euler Deconvolution among others (Reid *et al.,* 1990; Oyeniyi *et al.,* 2014; Oladele and Ayolabi, 2014). These methods rely on simple applications of calculus and Fourier transformations to enhance edges of spatial field signals (Reid *et al.,* 1990; Balogun, 2019).

Linear geologic structures are important surface/subsurface features with a lot of significance (Abdullah *et al.,* 2013). Being potential host for the accumulation of groundwater, they are the major structure of interest in ground water prospecting (Ejepu *et al.,* 2017). However, in construction works, they are avoided as much as possible (Amadi *et al.,* 2012).

One of the most significant pieces of information needed for planning in pre-construction site studies where geophysics is gradually growing to become a reliable, fast, cost-effective, and non-invasive tool, is the knowledge of orientation, distribution, and deep extent of linear geologic features (Isaksson *et al,* 2017; Adewumi and Olorunfemi, 2005). In most situations where pre-construction site research studies were deemed unnecessary, avoidable structural flaws are often discovered and a large amount of money wasted (Mattsson and Wahlgren, 2010). To avoid this

wastage and risk pose to lives, major construction companies have begin to spend in pre-construction studies that include geophysical mapping of linear geologic features, many of which could be harmful to engineering constructions.

Magnetic method has been successfully employed in the mapping of geological structures for the purpose of construction and ground water prospecting both in sedimentary and basement complex terrains. One of such studies where magnetic method was used is the work of Oladejo *et al.,* (2020), where high resolution magnetic data of the sedimentary terrain and part of the basement complex of Southwestern Nigeria were processed and interpreted to provide fault architecture of the area. It represents a good case study for the applicability of magnetic method in mapping geologic structure both within the sedimentary terrain and basement complex environment.

Another case study where aeromagnetic mapping was used in the delineation of lithological structures is the work of Okpoli and Oludeyi (2019). The total magnetic intensity field data was reduced to the magnetic equator, regional and residual fields were separated, before suites of enhancement techniques which include upward and downward continuation, tilt derivative, second vertical derivative, analytical signal, and Euler deconvolution were used to enhance the data for easy delineation of linear magnetic structure.

Electrical resistivity prospecting method can also be useful and reliable in delineating linear geologic structures. In order to improve the credibility of the results obtained from magnetic data, other geophysical methods like the electrical resistivity method can be deployed so as to give much confidence and confirm the structures delineated by the magnetic method (Okunubi and Olorunfemi, 2016; Oni *et al.*, 2020).

Depending on the technique and array adopted, electrical resistivity method can aid in revealing the two-dimensional image of the subsurface, which is often good for identifying vertical and near-

vertical geologic structures such as faulted and fractured zones, shear zones, defining basement/bedrock topography, identifying basement depressions, and delineating various sorts of other geological features. The reliable image of the subsurface derivable from 2D electrical resistivity survey may have influenced the increased use of two-dimensional imaging techniques in groundwater and engineering studies (Chirindja *et al.,* 2017; Olorunfemi and Oni, 2019; Olorunfemi *et al.,* 2020; Olorunfemi *et al.,* 2021).

Ozegin *et al.,* (2013) adopted the double-dipole array of the 2D electrical resistivity imaging to investigate a building site in a basement complex environment in South-South Nigeria with the aim of determining whether or not the subsurface is suitable for building construction. The result from the pseudo-sections delineated four distinct geologic strata which were basically clayey topsoil, sandy clay/highly weathered layer, weathered/fractured basement and fresh basement. Some geologic structures suspected to be fault were observed on the pseudo-sections.

A case study where integration of aeromagnetic map and electrical resistivity method was used in the delineation of geologic structures in proposed construction sites was presented in the work of Aina et al. (1996) at two sites across the Katsina-Ala River in the Katsina-Ala Local Government of Benue State, Nigeria. The objectives of the studies were to determine bedrock depths, bedrock relief, delineate geologic structures, the type of the superficial deposits overlying the bedrock in order to determine the most suitable locations for the potential minor and major axis for hydroelectric dams.

1.6 Research Methodology

High resolution aeromagnetic data of the region (Sheet 279 – Ilaro Sheet) where the study area is located was procured from Nigerian Geological Survey Agency (NGSA) and the study area was "windowed out" for localised processing operations.

Near-surface (cultural) noises were first filtered using the upward continuation approach. The data were subsequently reduced to the magnetic equator using the "Reduction to the Magnetic Equator (RTE)" filter operator. This was done in order to reposition anomalies at magnetic low latitude to appear as if there were actually acquired at zero magnetic inclination so that interpretation will be less ambiguous.

The "Reduced to the Magnetic Equator" TMI data were decomposed into residual and regional field components and the residual field was enhanced using the Total Horizontal Derivative (THD), Euler Deconvolution and Tilt Derivative (TDR) enhancement operations for proper delineation of the magnetic linear structures. The delineated lineaments were extracted and presented in as the magnetic lineament map. 2D Electrical Resistivity Tomography (ERT) data were subsequently acquired within the study area and the result integrated with the result of the magnetic data and interpreted.

1.7 Limitation of the Study

Accessibility was restricted during the 2D ERT survey due to the presence of a large forested swamp. This restricted the occupation for the 2D ERT survey mainly to the western and central parts of the study area.

1.8 Expected Contribution to Knowledge

The study will reveal the locations of plausible linear geologic structures and their density and orientation at the Mountain Top University's permanent site in Makogi-Oba, Ibafo, Ogun State, Nigeria.

CHAPTER TWO

BASIC THEORY OF THE METHODS USED

2.1 Basic Principles of Magnetics Method

Within the vicinity of a bar magnet, magnetic flux is developed which flows from one end of the magnet to the other (Figure 2.1). This flux can be mapped from the directions assumed by a small compass needle suspended within it. The points within the magnet where the flux converges are known as the poles of the magnet (Telford *et al.,* 1990; Kearey *et al.,* 2002). A freely-suspended bar magnet similarly aligns in the flux of the earth's magnetic field. The pole of the magnet which tends to point in the direction of the earth's north pole is called the north-seeking or positive pole, and this is balanced by a south seeking or negative pole of identical strength at the opposite end of the magnet (Lowrie, 2007). The force, **F**, between two magnetic poles of strength m_1 and m_2 separated by a distance, r, is given by

$$\mathbf{F} = \frac{\mu_0 m_1 m_2}{4\pi\mu_R r^2} \qquad 2.1$$

where μ_0 and μ_R are constants corresponding to the magnetic permeability of vacuum and the relative magnetic permeability of the medium separating the poles.

The force is attractive if the poles are of different sign and repulsive if they are of like sign. The magnetic field **B** due to a pole of strength *m* at a distance, r, from the pole is defined as the force exerted on a unit positive pole at that point by:

$$\mathbf{B} = \frac{\mu_0 m}{4\pi\mu_R r^2} \qquad 2.2$$

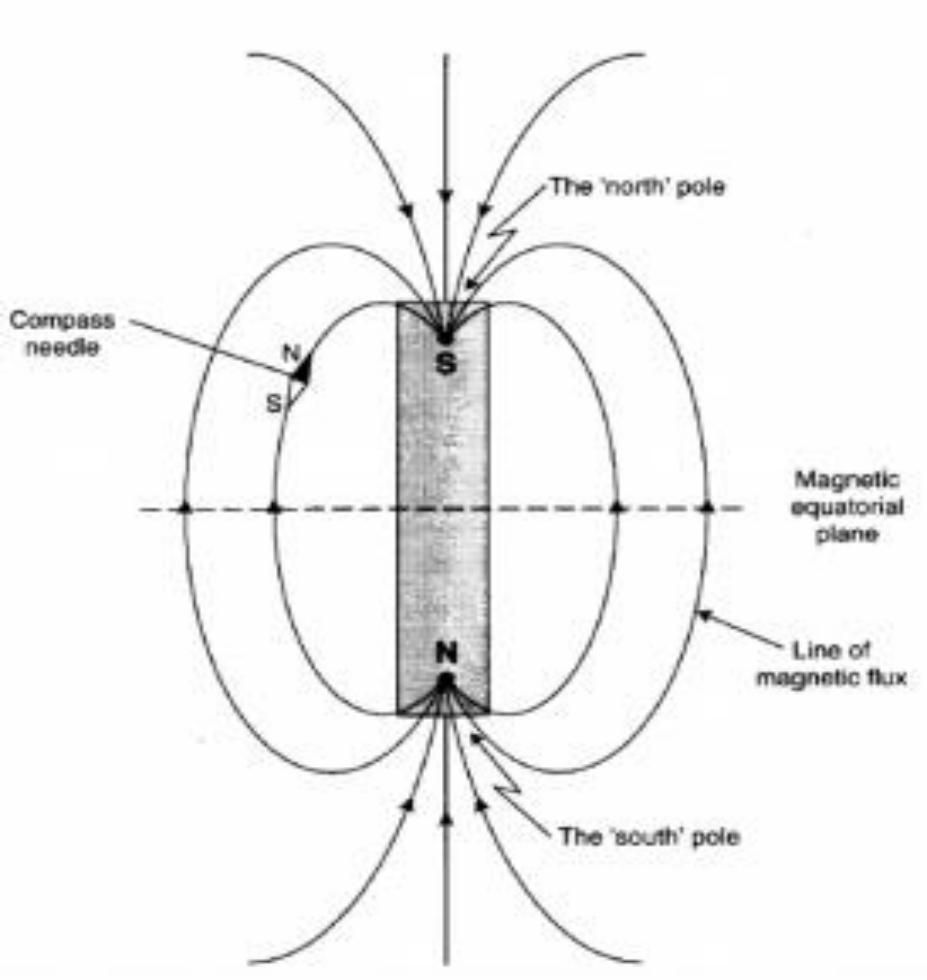

Figure 2.1: Magnetic Flux Surrounding a Bar Magnet (Telford *et al.*, 1990)

Magnetic fields can be defined in terms of magnetic potentials in a similar manner to gravitational fields. For a single pole of strength, *m*, the magnetic potential, *V*, at a distance, r, from the pole is given by Reynolds (1997) as:

$$V = \frac{\mu_0 m}{4\pi\mu_R r} \qquad 2.3$$

The magnetic field component in any direction is then given by the partial derivative of the potential in that direction. In the SI system of units, magnetic parameters are defined in terms of the flow of electrical current. If a current is passed through a coil consisting of several turns of wire, a magnetic flux flow through and around the coil annulus which arises from a magnetizing force ***H*** (Reynold, 1997; Lowrie, 2007).

The magnitude of **H** is proportional to the number of turns in the coil and the strength of the current, and inversely proportional to the number of turns in the coil and the strength of the current, and inversely proportional to the length of the wire, so that **H** is expressed in Am^{-1}. The density of the magnetic flux, measured over an area perpendicular to the direction of flow, is known as the magnetic induction or magnetic field **B** of the coil. **B** is proportional to **H** and the constant of proportionality μ is known as the magnetic permeability. Lenz's law of induction relates the rate of change of magnetic flux in a circuit to the voltage developed within it, so that **B** is expressed in Vsm^{-2} also known as Weber (Wb) (Telford *et al.,* 1990; Reynold, 1997; Lowrie, 2007)

The unit Wbm^{-2} also designated as the tesla (T) is the unit of measurement in magnetic survey. Permeability is consequently expressed in Wb$A^{-1}m^{-1}$ or Henry per meter, Hm^{-1}. The c.g.s unit of magnetic field strength is the gauss (G), numerical equivalent to 10^{-4} T. The Tesla is too large a unit in which to express the small magnetic anomalies caused by rocks, and a subunit, the nanotesla (nT), is employed (1 nT = 10^{-9} T). The c.g.s system employs the numerically equivalent

gamma (γ), equal to 10^{-5} G. Common magnets exhibit a pair of poles and are therefore referred to as dipoles. The magnetic moment M of a dipole of strength, *m*, at a distance, *l*, of l m apart is given by:

$$\mathbf{M} = ml \qquad 2.4$$

The magnetic moment of a current-carrying coil is proportional to the number of turns in the coil, its cross-sectional area and the magnitude of the current, so that magnetic moment is expressed in Am^2. When a material is placed in a magnetic field it may acquire a magnetization in the direction of the field which is lost when the material is removed from the field (Telford *et al.*, 1990; Reynold, 1997; Lowrie, 2007). This phenomenon is referred to as induced magnetization or magnet polarization, and results from the alignment the material has magnetic poles distributed over its surface which correspond to the end of the dipoles.

According to Telford et al. (1990) and Lowrie (2007), the intensity of induced magnetization J_i of a material is defined as the dipole moment per unit volume of material.

$$\boldsymbol{J_i} = \frac{\boldsymbol{M}}{LA} \qquad 2.5$$

Where $\boldsymbol{M}$ is the magnetic moment of a sample of length, L, and cross-sectional area A. $\boldsymbol{J}_i$ is consequently expressed in Am^{-1}. In the c.g.s system intensity of magnetization is expressed in emu. cm^{-3} (emu= electromagnetic unit), where 1 emu.cm^{-3}= 1000 Am^{-1}.

The induced intensity of magnetization is proportional to the strength of the magnetizing forces **H** of the inducing field.

$$\boldsymbol{J_i} = \kappa \boldsymbol{H} \qquad 2.6$$

Where κ is the magnetic susceptibility of the material, since $\boldsymbol{J}_I$ and **H** are both measured in Am^{-1}. Susceptibility is dimensionless in the SI system. In the c.g.s system susceptibility is similarly dimensionless.

2.1.1 Magnetic Induction of Rocks

The magnetic induction, **B,** of a magnetic material such as a rock with positive magnetic susceptibility is given by the total field within the rock material which includes:

(a) the strength of the earth's magnetic field, $\mathbf{H}_i$, that the rock material is exposed to

(b) the strength of the magnetic field in the rock materials itself, **H**, arising from its being polarized from the exposure.

According to Blakely (1996), the field $\mathbf{H}_i$ is a product of the intensity of magnetization $\boldsymbol{J_i}$and a solid angle 4π

$$\boldsymbol{H_i} = 4\pi \boldsymbol{J_i} \qquad 2.7$$

$$\boldsymbol{B} = \boldsymbol{H} + \boldsymbol{H_i} = \boldsymbol{H} + 4\pi \boldsymbol{J_i} \qquad 2.8$$

Substituting equation 2.6 into equation 2.8, we have

$$\boldsymbol{B} = \boldsymbol{H} + 4\pi\kappa \boldsymbol{H} \qquad 2.9$$

$$\boldsymbol{B} = \boldsymbol{H}\ (1 + 4\pi\kappa) \qquad 2.10$$

The ratio of the magnetic induction **B** to the magnetizing field **H** is referred to as the magnetic permeability.

$$\mathbf{B}/\mathbf{H} = 1 + 4\pi\kappa = \mu \qquad 2.11$$

$$\mathbf{B} = \mu \boldsymbol{H} \qquad 2.12$$

"μ" is the magnetic permeability of the medium between the magnetizing field H and the rock material.

2.1.2 The Geomagnetic Field

The Earth's magnetic field is believed to originate in the core. Although the mechanism is uncertain, it is believed to be created by magneto-hydrodynamic processes (Self-excited dynamo theory) (Lowrie, 2007). It is currently believed that the geomagnetic field is generated by shearing and twisting fluid motions within the liquid, electrically conducting outer core, the result being a dynamo, which maintains and regenerate the earth's magnetic field (Reynold, 1997). It is believed that only 1% of the earth's magnetic field is due to sources outside the earth (atmosphere). The geomagnetic field is usually described by a bar magnet at the core, with the lines of magnetic force looping from the south magnetic pole to the north magnetic pole.

In practice, it is a little more complex with some multi-polar patterns, but to a first approximation the dipolar model is convenient. While the N-S magnetic polar axis is currently inclined at an angle of about 100^{o} to the earth's axis of rotation, it is thought that the magnetic and geographic poles would coincide when averaged over a long period of time.

2.1.3 The Geomagnetic Elements

The earth's magnetic field is a vector quantity; that is, it has both magnitude and direction. The magnitude of this field is relatively weak, with maximum intensity near the magnetic poles. The geomagnetic elements (Figure 2.2) are taken to be components parallel to the geographic north and east directions. From a geological point of view, there are two important types of measurement relating to the Earth's magnetic field.

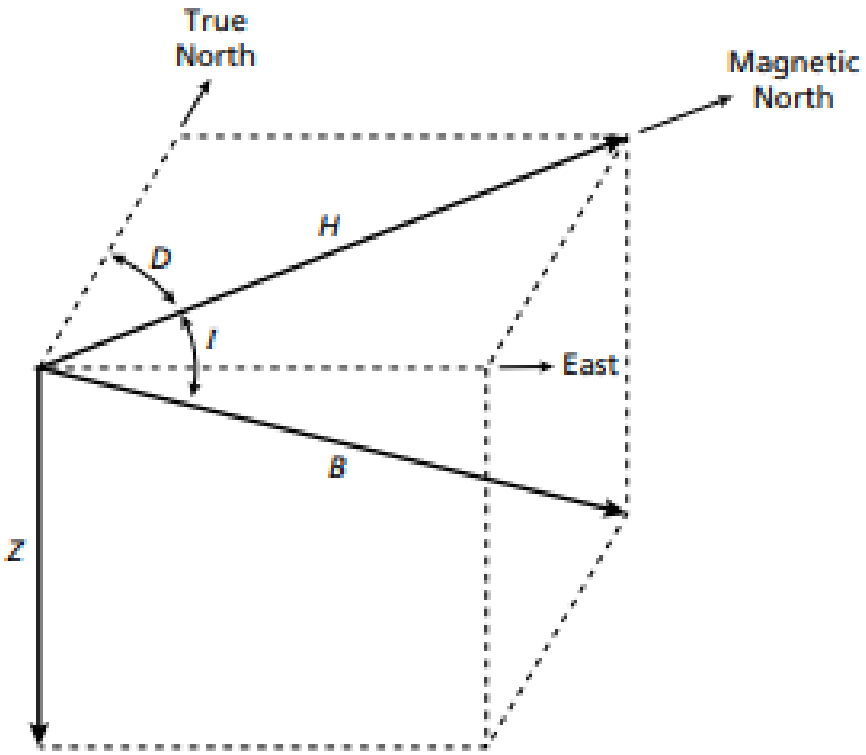

Figure 2.2: The Geomagnetic Elements (Telford *et al.*, 1990)

(a) The angle of declination (D) which is the angle between the observed compass reading (magnetic north) and the true north.

(b) The angle of inclination (I) which is the angle of dip of a magnetized needle relative to the horizontal. This angle varies from 90^o (vertical) at the magnetic poles to 0^o (horizontal) at the magnetic equator.

Inclination (I) is thus mathematically related to latitude (λ)

$$\text{Tan } I = 2 \tan\lambda \qquad 2.13$$

And consequently;

$$X^2 = Y^2 + Z^2 = F^2 \qquad 2.14$$

2.1.4 Aeromagnetic Survey

Majority of magnetic surveys are conducted in the air, with the sensor either towed in a 'bird' to shield it from the aircraft's magnetic field or placed in a 'stinger' in the aircraft's tail, in which case the inboard coil installations compensate for the aircraft's magnetic field. Aircraft usually employed for airborne magnetic surveys can either be a fixed-wing or rotary-wing (helicopter) aircraft. The rotary-wing (helicopter) is most suitable for rough terrain. Fixed-wing aircraft are less expensive, cover more ground faster, and produce higher-quality data in normal circumstances (Arora *et al.*, 2011).

2.1.4.1 Configuration System

Two basic sensor configurations are usually employed in airborne magnetic survey and are explained below;

1. The towed-bird Configuration

The sensor is placed far enough from the airplane in this configuration so that the magnetic field generated by the aircraft is minimal at the sensor. The towed-bird system produces excellent data at the low speeds typical of helicopter surveys, and it is the most popular configuration utilized in helicopter installations. The towed bird is subjected to platform (bird) motion and tow cable vibrations at the comparatively high speeds of fixed-wing aircraft (about 150 mi/h, or 240 km/h). The towed-bird installations are sometimes employed with fixed-wing aircraft. Figure 2.3 is a typical line plan for an airborne magnetic survey.

2. The Tail-stringer Installation.

The sensor is mounted on a stiff rod at the aircraft's back. The sensor is sometimes installed in a wingtip pod instead. A wingtip installation is similar to a tail-stinger design in terms of considerations. The tail-stinger mounting is the most prevalent option nowadays.

2.1.4.2 Instrumentation

The following are the essential instruments required for airborne magnetic survey

1. Stinger or towed-bird
2. Doppler Navigation System
3. Digital data acquisition system: Magnetometer, Altimeter, Time-synchronization device and GPS.
4. Analog Recorder: Used to record specific parameters, such as magnetics and altimeter data, for in-flight quality control and post-flight review.

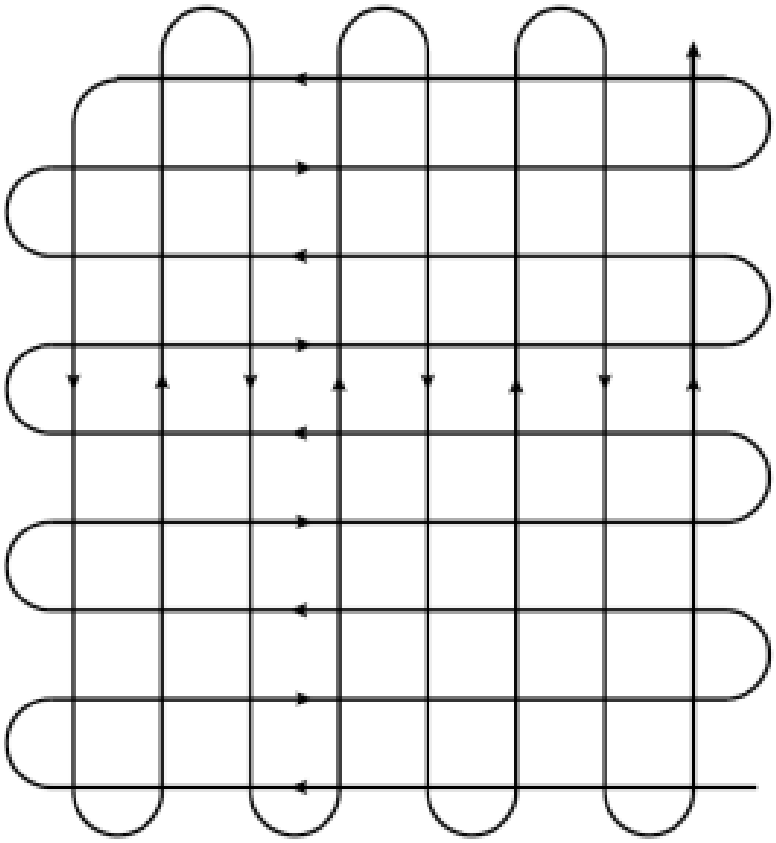

Figure 2.3: A typical flight plan for an aeromagnetic survey (Kearey, 1999)

5. Track Recovery System: A vertically mounted video camera or 35 mm film camera system that provides actual, visible track information in addition to the Doppler navigation system.
6. Magnetic Compensation Device (fixed-wing only): used for accounting for the aircraft's induced (both electrical and platform motion) and permanent magnetic fields.

Auxiliary equipment used in airborne magnetic survey include: inertial frame of reference compensating systems, other geophysical instruments such as multispectral scanners, gamma-ray spectrometers, active or passive EM (electromagnetic) systems and others. Ground support equipment includes a magnetometer and recording device at the base station and a field computer system.

2.1.4.3 Advantages of Aeromagnetic Survey

The following are the advantages of aeromagnetic survey.

1. Aeromagnetic surveying is quick and inexpensive, costing about 40% less per line kilometer than ground surveying.
2. Large areas can be quickly surveyed without incurring the expense of deploying a field party into the survey area.
3. Data can be gathered in regions that are inaccessible to ground survey.

2.1.4.4 Limitations of Aeromagnetic Survey

Position fixing used to be the most challenging difficulty in airborne surveys, but the availability of GPS has to a good extent resolved this problem.

2.1.5 Field Operational Problems

Either aeromagnetic, ship borne or ground magnetic survey, magnetic readings are usually affected by stray fields from iron and steel (cultural noise) most of which we cannot fully steer clear off during magnetic data acquisition. To eliminate this kind of noise, the noise is filtered from the aeromagnetic data by upward continuing the data to a moderate height of 80 m so that the cultural noises (which are known to be dominated by high wavenumber spectrums) can decay rapidly as we move higher away from the source.

2.2 Basic Principles of Electrical Resistivity Method

Electrical resistivity is a basic and diagnostic physical property that may be measured in earth materials using a variety of techniques (Kearey *et al.,* 2002). This method involves injecting a direct, artificially created current into the ground and measuring the potential difference that results at the surface (Telford *et al.,* 1990).

2.2.1 Elementary Theory

Consider a cylindrical wire of length (l) and cross-sectional area (A) carrying a current (I) (Fig.2.4).

The resistance $R \alpha \frac{L}{A}$

$$\text{or } R = \rho \frac{L}{A} \qquad 2.15$$

where the constant of proportionality ρ is the electrical resistivity. According to Ohm's Law.

$$R = \frac{\Delta V}{I} \qquad 2.16$$

where ΔV is the potential difference across the wire and I is the electric current through it. Combining equations 2.15 and 2.16 and re-arranging

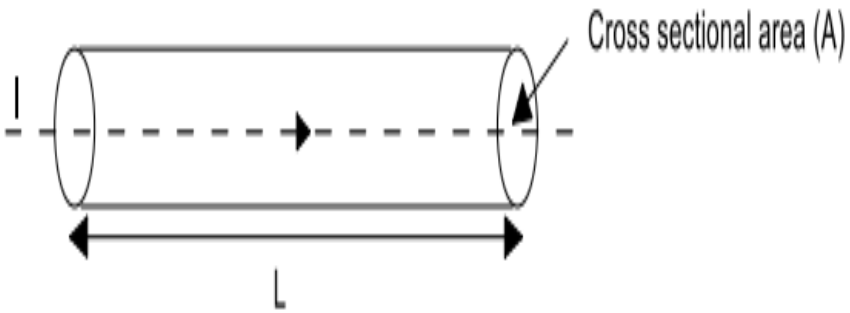

Figure 2.4: A Cylindrical Current Carrying Wire (Reynolds, 1997)

$$\rho = \frac{A\,\Delta\,V}{L\,I} \qquad 2.17$$

Equation 2.17 can be used to determine resistivity ρ of any homogeneous and isotropic medium provided the geometry is simple e.g. cylinder, parallel, pipes and cubes (Telford *et al.*, 1990; Kearey *et al.*, 2002)

2.2.2 Electrodes on the Surface of a Half Space

According to Telford et al., (1990), for a semi-infinite medium however the resistivity at every point must be defined. The parameters A and L of an element within the semi-infinite medium are shrunk to infinitesimal size;

$$\rho_r = \frac{\lim_{L \to 0} \frac{\Delta V}{L}}{\lim_{A \to 0} \frac{I}{A}} = \frac{E_l}{J} = \frac{E}{J} \qquad 2.18$$

Assuming that current enters a homogeneous whole space via an electrode placed at the origin "O" (Figure 2.5) where J is the current density and E is the electric field.

$$J = \frac{1}{\rho}\, E \; or \; \sigma E \qquad 2.19$$

The current flows radially from the origin "O" such that the current density at distance r, is

$$J_r = \frac{I}{A} = \frac{I}{4\pi r^2} \qquad 2.20$$

But from equation 2.19

$$J_r = \sigma\, E_r \text{ or } \frac{1}{\rho} E_r$$

$$E_r = J_r\, \rho = \frac{I\,\rho}{4\pi\, r^2} \qquad 2.21$$

But E_r is the gradient of a scalar potential

$$\text{or } E_r = -\,\Delta V \; or \; -\frac{dV}{dr}$$

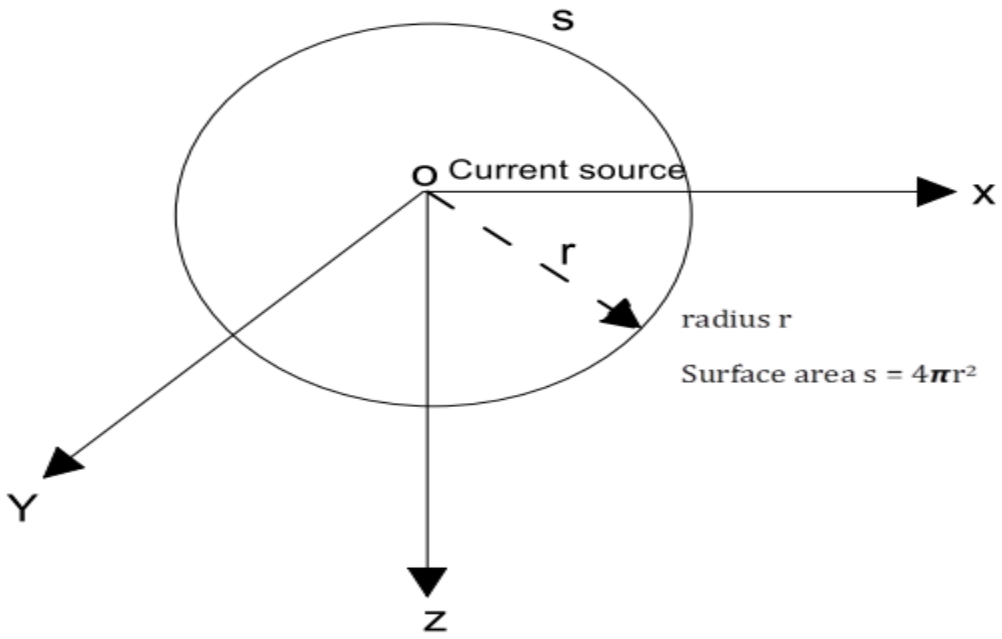

Figure 2.5: Current at the Centre of a Homogeneous Spherical Earth (Reynolds, 1997)

$$\int dV = \int -\frac{I\,\rho}{4\,\pi\,r^2}$$

$$V = \int_r^{\infty} -\frac{I\,\rho}{4\,\pi\,r^2} = \frac{I\,\rho}{4\,\pi\,r} \qquad 2.22$$

Equation 2.22 is the potential due to a single current source at the center of a spherical earth with radius r. Equation 2.22 is applicable in borehole geophysics during resistivity logging when current source is below the surface of the earth. In surface resistivity survey, current source is located at the surface of the earth (hemispherical earth or half space) (Figure 2.6).

The current density crossing the hemispherical surface is given as

$$J = \frac{I}{A} = \frac{I}{2\,\pi\,r^2}$$

$$J = \sigma E = \frac{I}{2\,\pi\,r^2}$$

Therefore, $E = \frac{I\,\rho}{2\,\pi\,r^2} and - \frac{dV}{dr} = \frac{I\,\rho}{2\,\pi\,r^2}$

$$\int dV = \int -\frac{I\,\rho}{2\,\pi\,r^2}\,dr$$

$$V = \frac{I\,\rho}{2\,\pi\,r} \qquad 2.23$$

Equation 2.23 is applicable in surface resistivity survey. It is the potential equation for two electrode array system, consisting of one current electrode and one potential electrode.

2.2.3 Four Electrodes at the Surface of the Earth

In electrical resistivity survey, four electrodes are used consisting of two current electrodes and 2 potential electrodes (Fig. 2.7).

The potential at $P1$ due to $C1$ and $C2$

$$V\rho_1 = \frac{I\,\rho}{2\,\pi}\left[\frac{1}{r_1} - \frac{1}{r_2}\right] \qquad 2.24$$

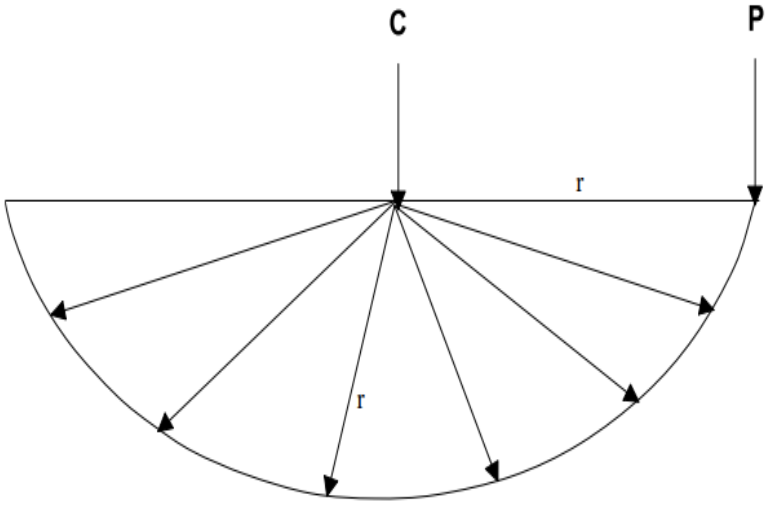

P = Potential Electrode

C = Current Electrode

Figure 2.6: Current Source at the Surface of the Hemispherical Earth (Reynolds, 1997)

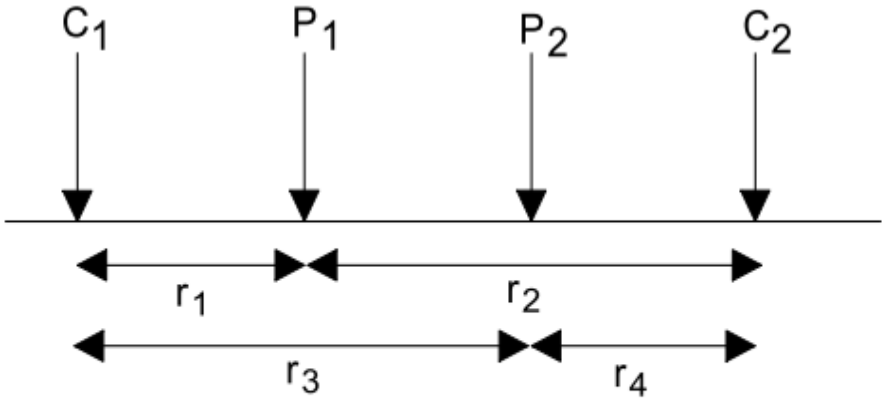

P_1, P_2 = Potential Electrode

C_1, C_2 = Current Electrode

Figure 2.7: Typical Four Electrode Array System (Reynolds, 1997)

The potential at $P2$ due to $C1$ and $C2$

$$V\rho_2 = \frac{I\,\rho}{2\,\pi}\left[\frac{1}{r_3} - \frac{1}{r_4}\right] \quad 2.25$$

Potential difference between $P1$ and $P2$ measured on the field

$$\Delta V = V\rho_1 - V\rho_2 = \frac{I\,\rho}{2\,\pi}\left[\frac{1}{r_1} - \frac{1}{r_2} - \frac{1}{r_3} + \frac{1}{r_4}\right]$$

$$\rho = \frac{2\,\pi\,\Delta V}{I}\left[\frac{1}{\left[\frac{1}{r_1} - \frac{1}{r_2} - \frac{1}{r_3} + \frac{1}{r_4}\right]}\right] \quad 2.26$$

Or $\rho = \frac{\Delta V}{I} G = RG$

where $G = 2\pi\left[\frac{1}{\left[\frac{1}{r_1} - \frac{1}{r_2} - \frac{1}{r_3} + \frac{1}{r_4}\right]}\right]$ 2.27

G is the geometric factor which depends upon the specific array used.

2.2.4 The Multielectrode System Configuration

The arrangement of electrodes in relation to each other is called the electrode configuration. Wenner, Schlumberger, dipole-dipole, gradient, pole-pole, pole-dipole and squared array are some of the array types that exist (Loke, 2002). Traditionally, all of these arrays make use a pair of current and potential electrodes, but technology has made it available that we can have numerous electrodes which are selected in pairs of current and potential electrode automatically. This is the concept of multielectrode system configuration. All the various array type used in traditional 2D electrical resistivity survey can also be engaged in the multielectrode system configuration. In this study the dipole-dipole array was adopted.

2.2.5 Instrumentation

The equipment required for resistivity survey include

- a power source (Transmitter)

- Multielectrode system resistivity meter (Supersting R8)
- Electrodes (112)
- Connecting cables
- Hammers

2.2.6 Limitations of Electrical Resistivity Method

The interpretation of a multiplayer sounding curve generally is not unique (Kearey *et al.,* 2002). This means that a given electrical sounding curve can correspond to a variety of subsurface distributions of layers' thicknesses and resistivities. Furthermore, several other limitations are inherent in the conventional methods of electrical sounding (Telford *et al.,* 1990; Kearey *et al.,* 2002). They are:

(i) Equivalence: This occurs in multi-layer resistivity curve. The curve can correspond to a great number of different geoelectric models. Commonest types of equivalence problem are:

   a. equivalence of K-type curves

   b. equivalent of H-type curves.

(ii) Monotonic change in resistivity: When the resistivity of the subsurface layer increases and decreases monotonically, the sounding curve may resemble a curve of a simple two-layer earth

CHAPTER THREE

MATERIALS AND METHODS OF STUDY

3.1 The Datasets

3.1.1 The Elevation Data

The elevation data adopted for the study is the high-resolution, Shuttle Radar Topographic Mission (SRTM) global elevation data (Digital Terrain Elevation Data – DTED®) having a spatial resolution of 30 m × 30 m and a near world-wide coverage. The data was acquired by radar interferometry and made use of the Earth's Gravity Model 1996 vertical datum. The unit of height measurement is metre (m) and the C-band wavelength is 5.6 cm.

3.1.2 The Aeromagnetic Data

The magnetic data used for the study is the high-resolution 100 m × 100 m grid aeromagnetic (Total Magnetic Field Intensity (TMI)) data, having a mean terrain clearance of 80 m and recording interval of 0.1 s, acquired by the Nigerian Geological Survey Agency between 2003 and 2010. For this study, the data was reduced to the magnetic equator to remove asymmetries associated with low magnetic latitude anomalies. The regional field was removed and the resulting residual field was processed and analysed.

3.1.3 The 2D Electrical Resistivity Tomography (ERT) Data

Four 2D ERT lines were acquired from the western to central part of the study area as much as accessibility can allow. The lines were positioned to intercept lineament delineated from aeromagnetic data so that results from both the aeromagnetic data and 2D ERT can be integrated. The 2D ERT data was acquired using "SuperSting R8" earth resistivity meter which is a resistivity/IP meter, having 112 electrodes. The Dipole-Dipole array was used and the electrode

spacing adopted was 10 m. The total spread length was 1110 m and the depth penetrated was 220 m. The 2D ERT data acquisition survey line plan is shown in Figure 3.1.

3.2 Methods of Study

3.2.1 Georeferencing and Digitisation the Analogue Site Map

The site map in form of an analogue survey plan was retrieved from the office of the Vice-Chancellor. The map was scanned, georeferenced and digitised. The coordinate system adopted in developing the analogue survey plan (i.e. UTM Zone 31N with reference to WGS '84 Datum) was noted and was maintained while georeferencing and digitising the analogue map. The software used for both the georeferencing and digitisation is the Surfer Surface Mapping System Software, version 12.0.626 from Golden Software, Inc, Colorado, United States of America.

Using the digitised values and coordinate system, a base map was developed for the study (Figure 1.1). Also, the digital terrain elevation data were gridded using the same software (Figure 1.2).

3.2.2 Processing of the Aeromagnetic Data

The aeromagnetic data were processed using the Geosoft's Oasis Montaj^{TM} software version 6.4.2 (HJ). The suites of basic data enhancement operations which include the least square polynomial fitting approach of regional-residual field separation, total horizontal derivative, Euler deconvolution and the tilt derivative, performed on the data with the Oasis Montaj^{TM} software are discussed below.

3.2.2.1 Least Square Polynomial Fitting

This technique was first suggested for use for regional-residual field separation in potential field data processing by DeLury (1950) and was used by Oldham and Sutherland (1955). It was later modified by Grant (1957). The theory is summarized below.

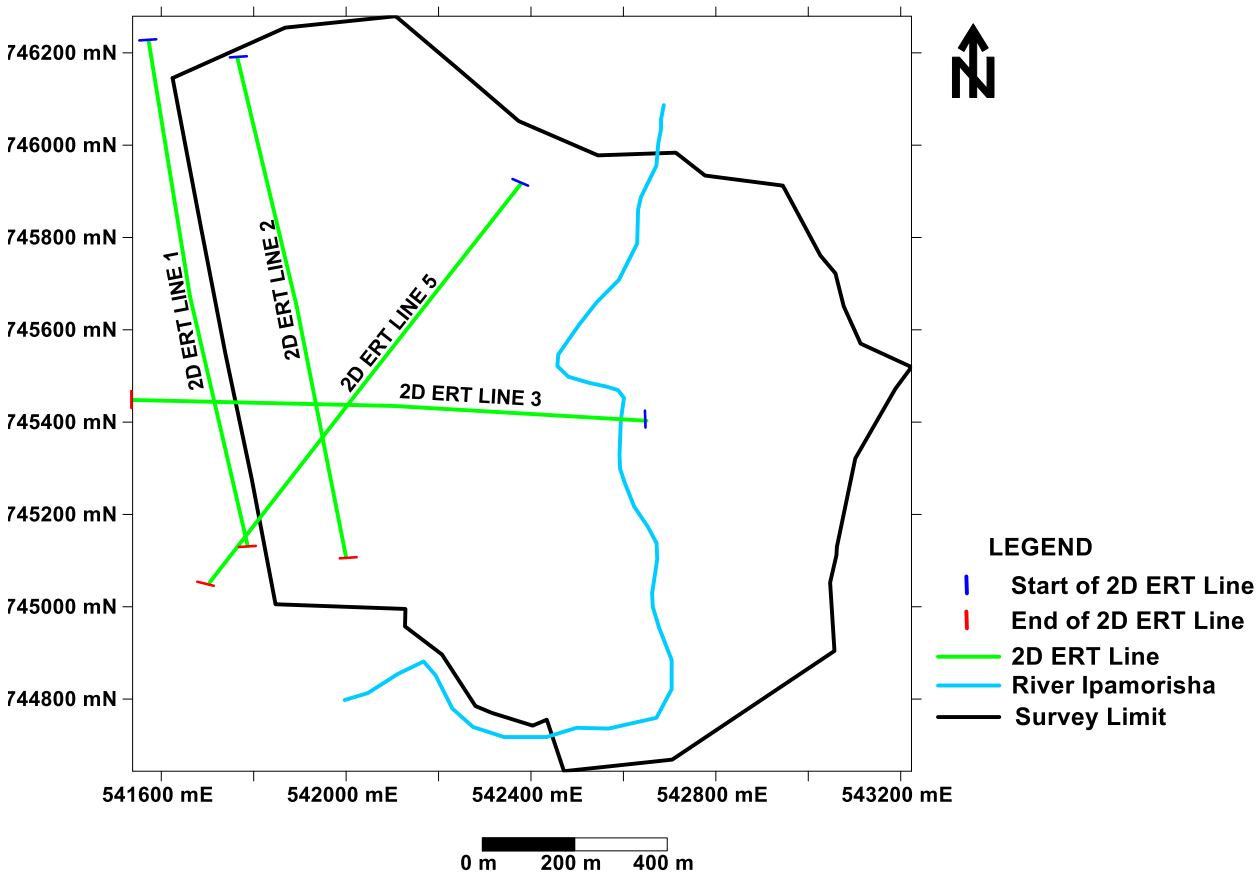

Figure 3.1: Base Map of the Study Area Showing the 2D ERT Profiles

Let the observed magnetic field T (x, y) be composed of a regional field T_R (x, y) and a residual field T_L (x, y) component.

Then

$$T(x, y) = T_R(x, y) + T_L(x, y) \quad 3.1$$

Let T_L be a random variable with zero mean and constant variable σ^2. Let the observed anomaly T be expressed in terms of two orthogonal polynomials of degree p and q (i.e $f_p(x)$ and f_q (y)) so that

$$T(x, y) = a_{00}f_0(x)f_0(y) + a_{10}f_1(x)f_0(y)$$

$$a_{01}f_0(x)f_1(y) + \cdots$$

$$a_{pq}f_p(x)f_q(y) \quad 3.2$$

where constant a_{rs} are determined by the least square techniques using the equation

$$a_{rs} = \frac{[s\{T(f_{r(x)})(f_s(y))\}}{S\{f_r^2(x)\}S\{f_r^2(y)\}} = \frac{T_{rs}}{p_r p_{s1}} \quad 3.3$$

3.2.2.2 Total Horizontal Derivative

This is a very efficient operation, applicable to potential field data, commonly used to accentuate edges of structures. The principle is based on the fact that the gradient of a function will be peak at a discontinuous point. Therefore, when we differentiate a potential field function such as the gravity and magnetic fields, where the derivative is peak is usually representative of a discontinuous point or zone. The total horizontal derivative is given in equation 3.4 below as

$$\text{THD} = \sqrt{(\frac{\delta T}{\delta X})^2 + (\frac{\delta T}{\delta y})^2} \quad 3.4$$

Where $\frac{\delta T}{\delta X}$ is the derivative of the magnetic field in the "x: direction, and $\frac{\delta T}{\delta y}$ is the derivative of the magnetic field in the "y" direction.

3.2.2.3 The Euler Deconvolution

Euler deconvolution operation is a very efficient edge enhancement technique in potential field data processing. It is widely used because it requires only little prior information about anomaly source geometry and requires no information about anomaly source vector in the case of magnetic anomalies (Reid *et al.,* 1990; 1980; Balogun *et al.,* 2016; Balogun, 2019).

One major important advantage of Euler deconvolution is that it gives the estimate of the depth of magnetic sources in addition to defining their edges. The Euler Deconvolution operation is based on solving Euler's homogeneity equation given in equations 3.5 and 3.6 as

$$(\text{x-}\ x_0)\frac{\delta T}{\delta \chi} + (\text{y-}\ y_0)\frac{\delta T}{\delta y} + (\text{z-}\ z_0)\frac{\delta T}{\delta z} = \eta\ (\beta - T) \quad 3.5$$

$$x\frac{\delta T}{\delta \chi} + y\frac{\delta T}{\delta y} + z\frac{\delta T}{\delta z} + \eta T\ = x_0\frac{\delta T}{\delta \chi} + y_0\frac{\delta T}{\delta y} + z_0\frac{\delta T}{\delta z} + \eta\beta \quad 3.6$$

where β is the regional value of the potential field and $x_0, y_{0,} z_o$ defines the position of the source, which produce the total potential field T measured at (x, y, z), η is the structural index.

3.2.2.4 Tilt Derivative

A generalized definition for the local phase of a potential field function is known as the tilt derivative (or angle). Due to the efficient Automatic Gain Control (AGC) enforced by the arc tangent function, which restricts the tilt angle to within the range -90 to +90 independent of the amplitude or wavelength of the magnetic field, mapping the magnetic tilt angle offers the advantage of magnifying weak magnetic anomalies (Verduzco *et al.,* 2004).

Tilt derivative is used to estimate the location and depth of magnetic sources. It is based on a model of a buried 2D vertical contact and it is a very straightforward way to estimate the location and strike of geological contact/faults, as well as the depth to basement of magnetic anomalies (Fairhead *et al.,* 2009). Depths to a magnetic source are estimated by taking the average of the distance between +45^{o} and -45^{o} contour lines (Verduzco *et al.,* 2004; Salem *et al.,* 2007; Balogun, 2019). Tilt derivative is expressed mathematically as

$$\text{TDR} = tan^{-1}\frac{VDR}{THD} \qquad 3.7$$

where VDR is the first vertical derivative and THD is the total horizontal derivative of the TMI respectively.

3.2.3 2D Electrical Resistivity Tomography (ERT) Data Processing

In order to process the 2D ERT data, Advance Geophysical Incorporated (AGI)'s "EarthImager software" was used to invert the data. Inversion of this kind is usually done by comparing the field measured data (model) with a corresponding theoretical model in order to generate an apparent resistivity inverted section (a solution) from the theoretical model that fits the measured field data. The difference between the field measured data and the corresponding theoretical model is expressed as the RMS error. The lower the RMS error, the higher the level of confidence in the result given by the inverted apparent resistivity pseudo-section generated.

3.2.4 Integration of Aeromagnetic and the 2D ERT Data

The Aeromagnetic and 2D ERT data were integrated so as to determine if lineaments delineated from aeromagnetic data can be confirmed from the 2D ERT results. If confirmed by both the results of the magnetic and electrical resistivity methods, a delineated lineament has thus been proved to exist within the subsurface beyond reasonable doubt.

CHAPTER FOUR

4.1 The Total Magnetic Intensity (TMI) Field, Reduced to the Magnetic Equator (RTE) TMI and the Residual Magnetic Intensity Maps

4.1.1 The Total Magnetic Intensity (TMI) Field Map

The TMI map was observed to be dominated by elongated to linear magnetic anomalies trending mostly in the approximate N – S direction, with just a few trending in the approximate East – West direction (Figure 4.1). In general, the whole region showed four magnetic field intensity zones (Labeled A, B, C and D), which are characteristically distinct with magnetic intensity decreasing from West to East (Figure 4.1). Though, all the zones appear to be linear, they vary in shape and size. It should also be noted that magnetic relief across this whole region is rather low, being just 2.6 nT in value.

The study area (i.e. Mountain Top University's permanent site) lies predominantly within the highest (pink colouration) and intermediate (yellow and green) intensity zones (Figure 4.1). The pattern of the decreasing magnetic intensities eastwards seems to be suggestive of a step-faulting phenomenon with depth to the faulted block decreasing eastwards. It should also be noted that since the study area is located in a magnetic low latitude region, magnetic lows on the map represent bodies or structures having relatively higher magnetic susceptibility while the magnetic highs represent bodies or structures with relatively lower magnetic susceptibility.

4.1.2 Reduced to the Magnetic Equator (RTE) TMI Field

In an attempt to reduce some of the ambiguities that may be associated with magnetic data interpretation, especially the ambiguity due to magnetic inclination, the data was reduced to the

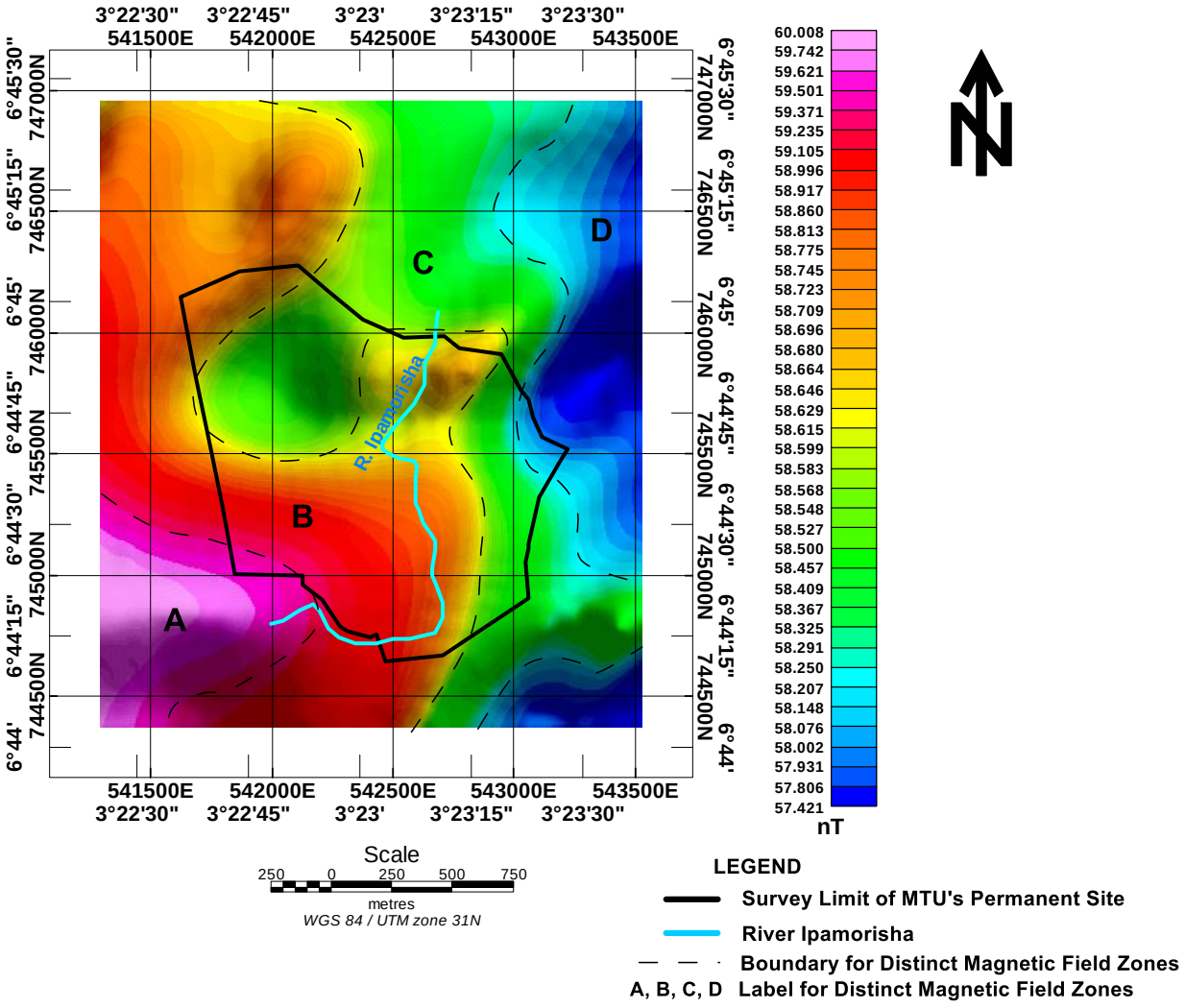

Figure 4.1: The Total Magnetic Intensity Field Map

magnetic equator so that the resultant magnetic data can appear as if it were acquired at the magnetic equator. The advantage of this is that "magnetic inclination" asymmetry associated with anomalies can be removed and any form of enduring asymmetry can be considered as due to the attitude of the causative body.

Due to the fact the study area is close to the magnetic equator (magnetic inclination and declination at the place being -13.598^{o} and -1.669^{o} respectively), there was no significant observable difference between the TMI field map (Figure 4.1) and the RTE field map (Figure 4.2). The interpretation of both maps is essentially the same.

4.1.3 The Residual Field Map

First order regional field was removed from the RTE map to generate the first order residual field map (Figure 4.3). The residual field map was observered to comprise of both elongated and spherical magnetic anomalies, some with relatively high magnetic intensities while some have relative low magnetic intensities.

The northcentral to northeastern, southwestern and southeastern regions were dominated by elongated, relatively high magnetic field intensity anomalies. The northwestern part is made up of roughly spherical, relatively low magnetic intensity anomalies and the "central eastern" and southern parts are made-up of elongated but also relatively low magnetic anomalies. An intersection of magnetic lows (labeled "Y") in the eastern part of the study area suggests the possibility of the study area being a shear zone (Figure 4.3). When the TMI map (Figure 4.1) was compared with the residual map (Figure 4.3), it was found out that the residual map has accentuated the short wavelength structures and suppressed the long wavelength structures dominating the TMI map significantly. Figure 4.4 shows the first order regional field removed from the RTE in the process of generating the residual map.

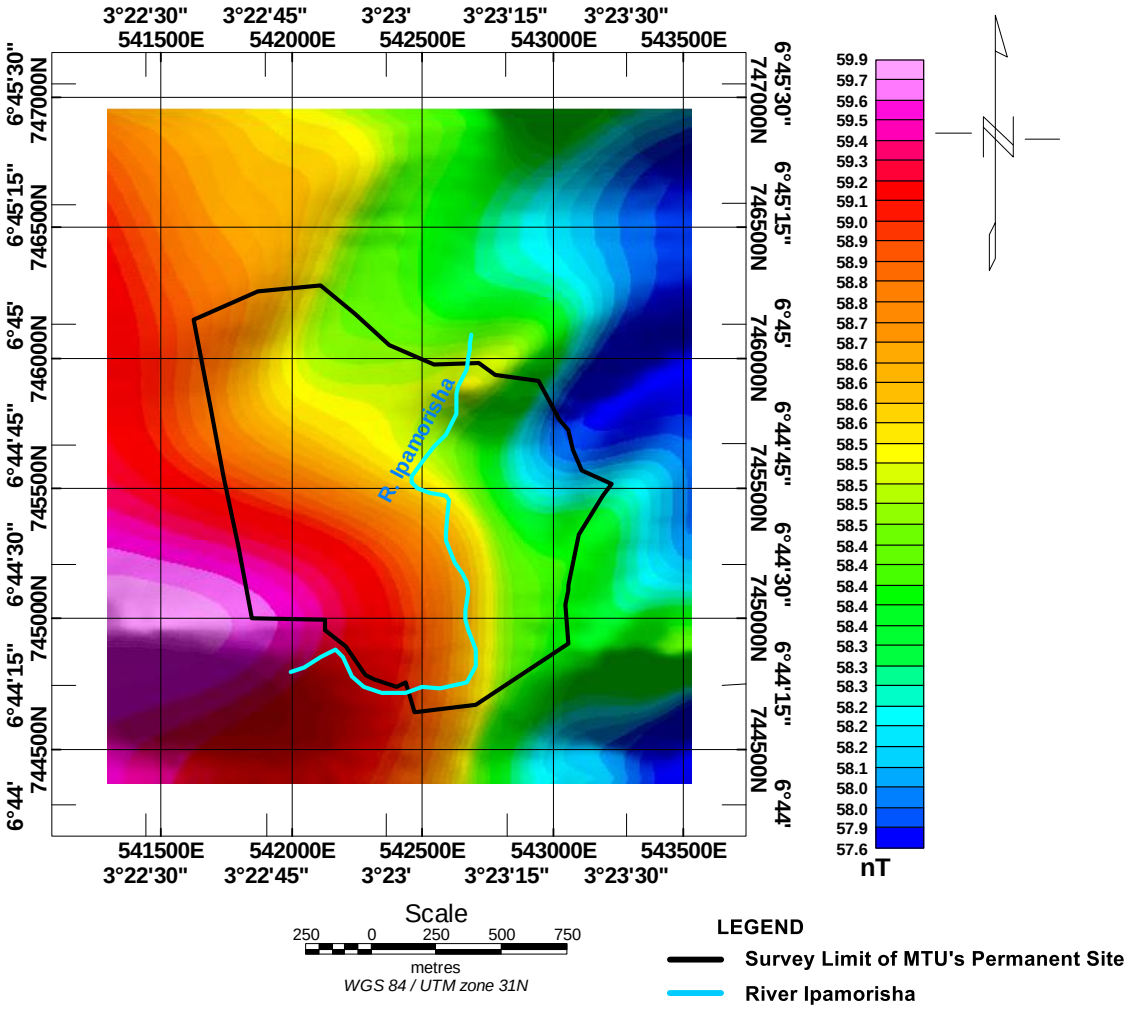

Figure 4.2: The Reduced to the Magnetic Equator TMI Map

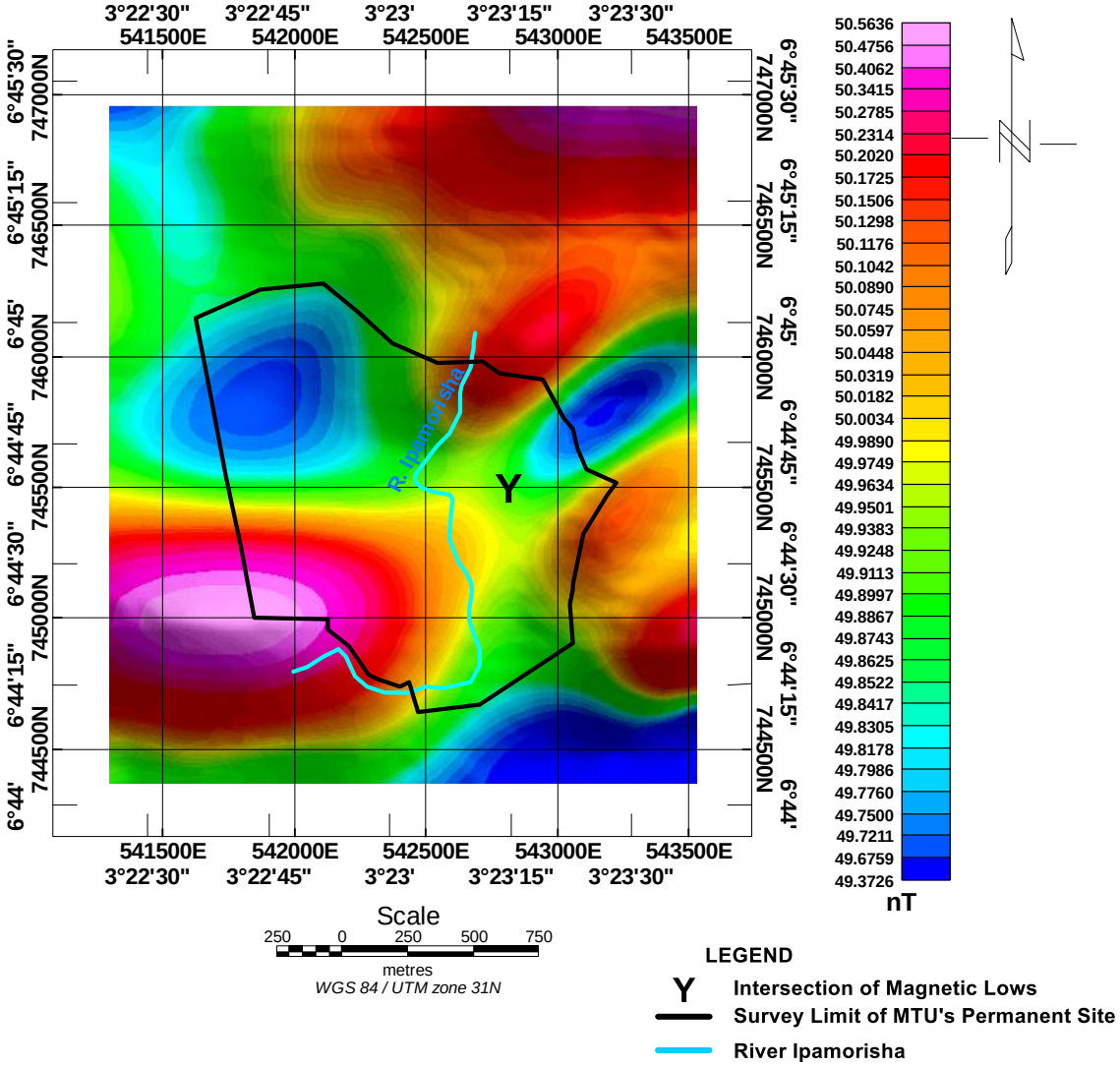

Figure 4.3: The Residual Field Map of the Study Area

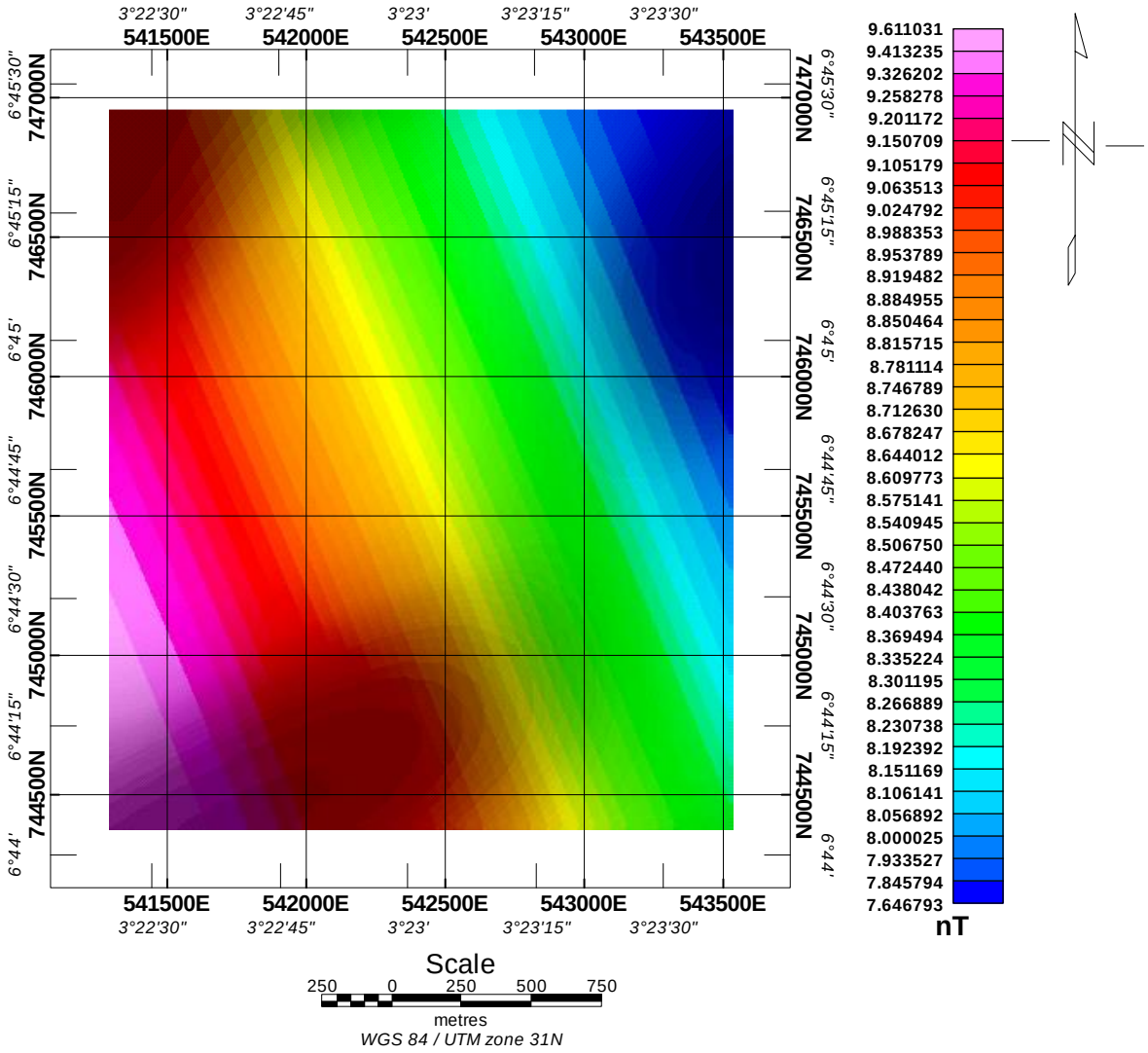

Figure 4.4: The Regional Field Map of the Study Area

4.2 Lineament Extraction

A combination of the Total Horizontal Derivative (THD), Euler Deconvolution and Tilt Derivative enhancement operations were employed for the delineation of geologic lineaments present in the study area. In geologic terms, these lineaments, where they are genuinely mapped usually indicate rock or lithologic contacts and fractures (i.e rock joints and faults).

4.2.1 Total Horizontal Derivative

From the knowledge of the application of differential calculus, it can be established that the gradient of a function will be maximum at a region where there is an abrupt change or where discontinuity of the function is observed. In similar terms, we expect that when we perform the first order horizontal derivative of a potential field function such as gravity and magnetic field with respect to their areal extent, the regions of peak gradient (derivative) should indicate regions of discontinuity of such field and this in geological terms will be suggestive of linear geologic structures.

Total horizontal derivative was performed on the residual field data and fifteen (15) long to intermediate scaled lineaments (or curvilineaments) and several other local (short) scaled lineaments were delineated (Figures 4.5(a) and (b)).

A conspicuous wide zone of structural weakness (labeled A), bounded to the West amd East by curvilineaments “2” and “3” respectively was delineated. The zone, covering most of the northwestern region where it has a width of 769.23 km, runs southwards, following the NW – SE trend initially before it changed course to continue due south and eventually terminating at the southeastern region where it thinned out to become only 128.2 m wide.

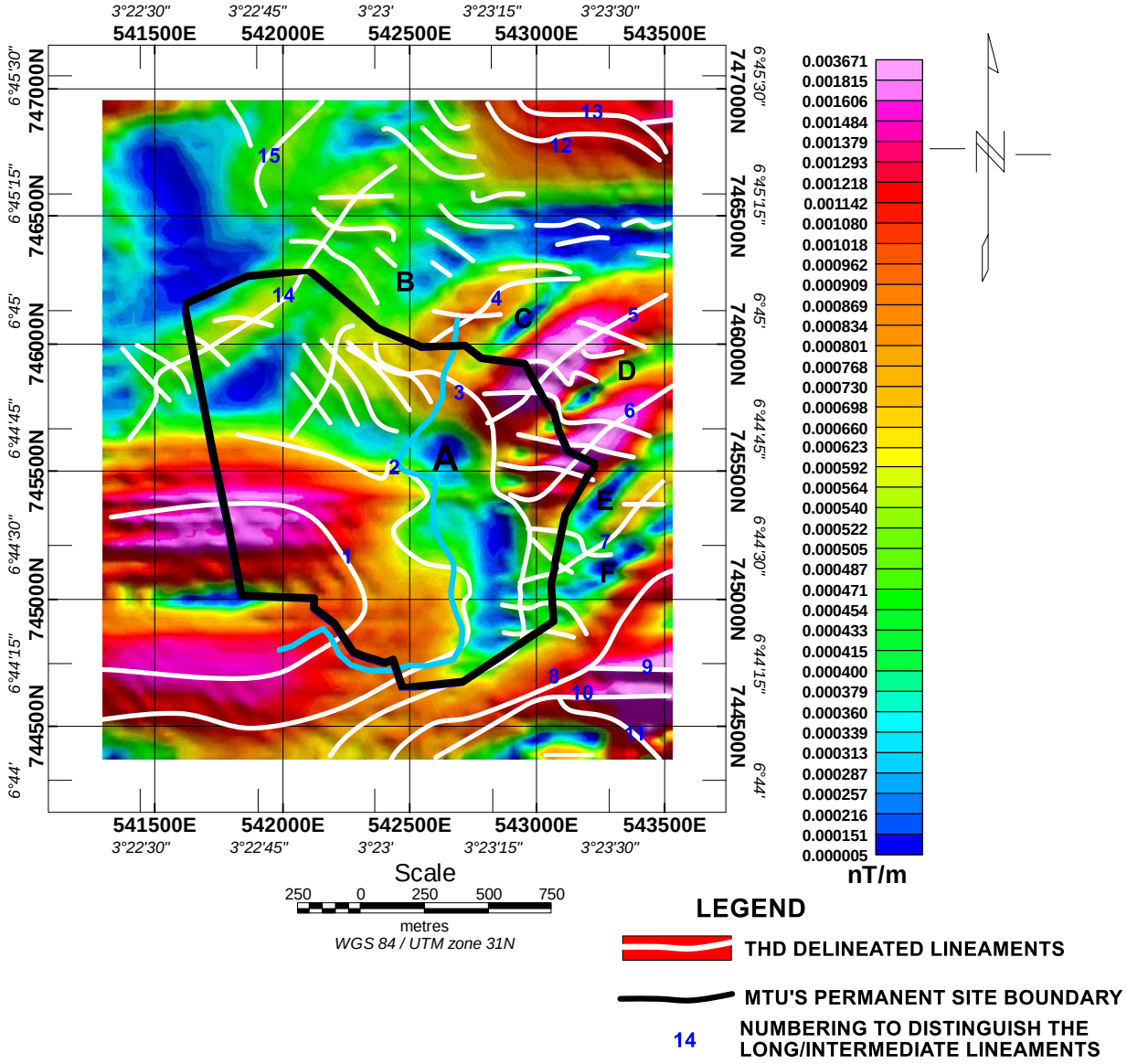

Figure 4.5(a): The Total Horizontal Derivative Map of the Study Area

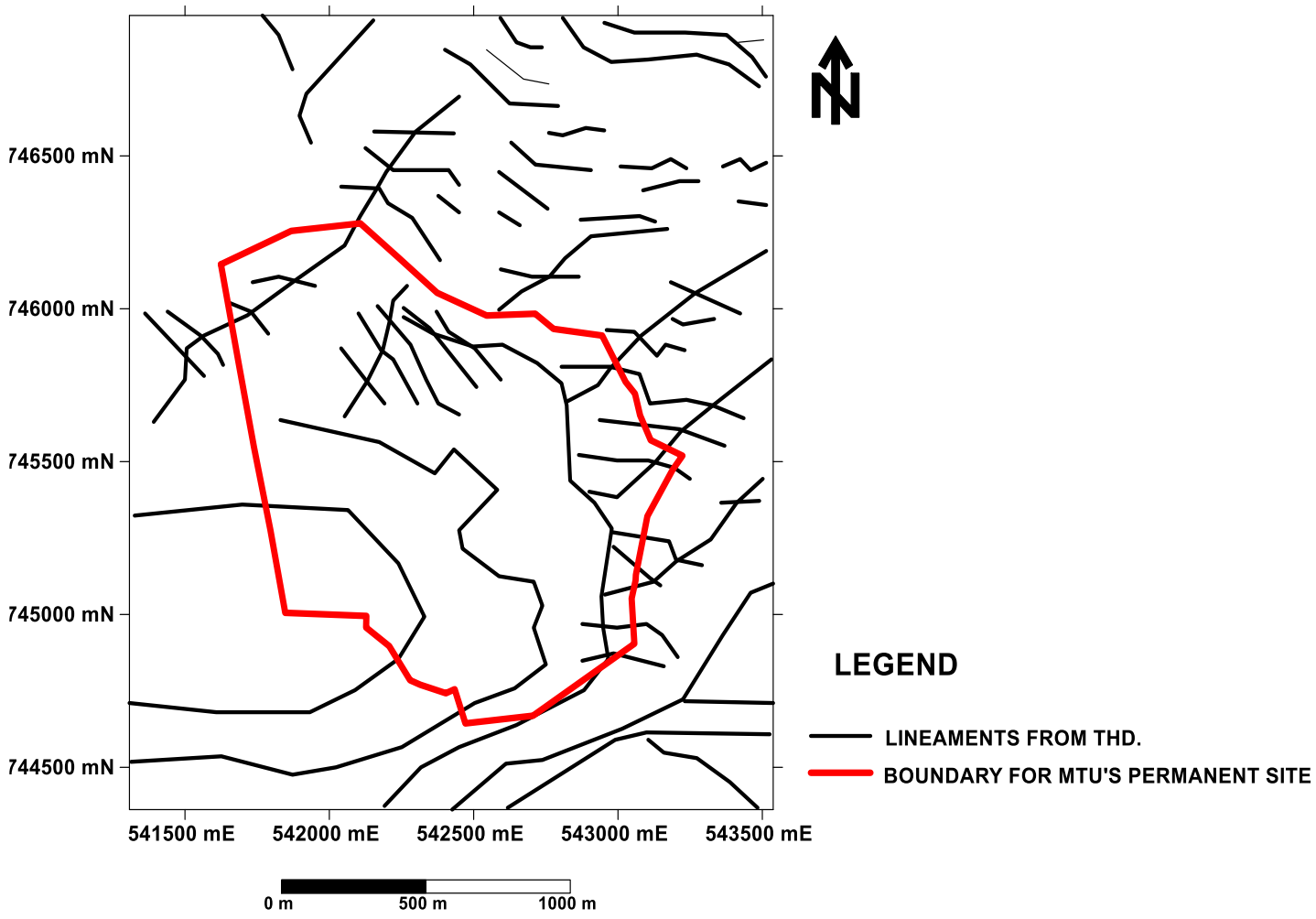

Figure 4.5(b): The Lineaments Delineated from Total Horizontal Derivative Operation

Five other zones of weakness, namely, B, C, D, E and F were observed at the eastern part of the study area. These zones are approximately parallel to one another and all trend in the approximate NE – SW direction. C, bounded by lineaments 4 and 5; D, bounded by lineaments 5 and 6; E, bounded by lineaments 6 and 7; and F, bounded by lineaments 7 and 8 all appear to terminate on curvilineament 3 and do not cut into Zone A. Only "Lineament 14", bounding Zone B to the west, cuts into Zone A signifcantly.

From the cross-cutting relationship, three tectonic events can be established based on the imprints left behind. The oldest is a first NE-SW trending event that formed the zones of weakness C, D, E and F. The second is the approximate NW-SE event that brought about the zone of weakness A which cut through structures C, D, E and F. The last observable event is also a NE-SW trending event, significantly represented by "Lineament 14" that cuts through Zone A at the northwestern end of the permanent site (Figure 4.5 (a)). It is most likely the youngest of all the events. The severe deformation observed in the study area presents the study area as a shear zone.

4.2.2 Euler Deconvolution

Euler deconvolution solutions for the data were obtained using the Euler's homogeneity equation presented in equation 3.6 and the solutions were plotted as color ranged symbols in Figure 4.6. Since the scope of the work is to delineate linear geologic strucures, a structural index of zero, representing the model for linear geologic structures, was adopted for generating the solutions.

It was discovered that only the long and intermediate ranged lineaments were well resolved by the Euler Deconvolution solution plot (Figures 4.6(a) and 4.6(b)). The plot presents most of the lineaments to have depths that rarely exceeds 200 m except at some few locations.

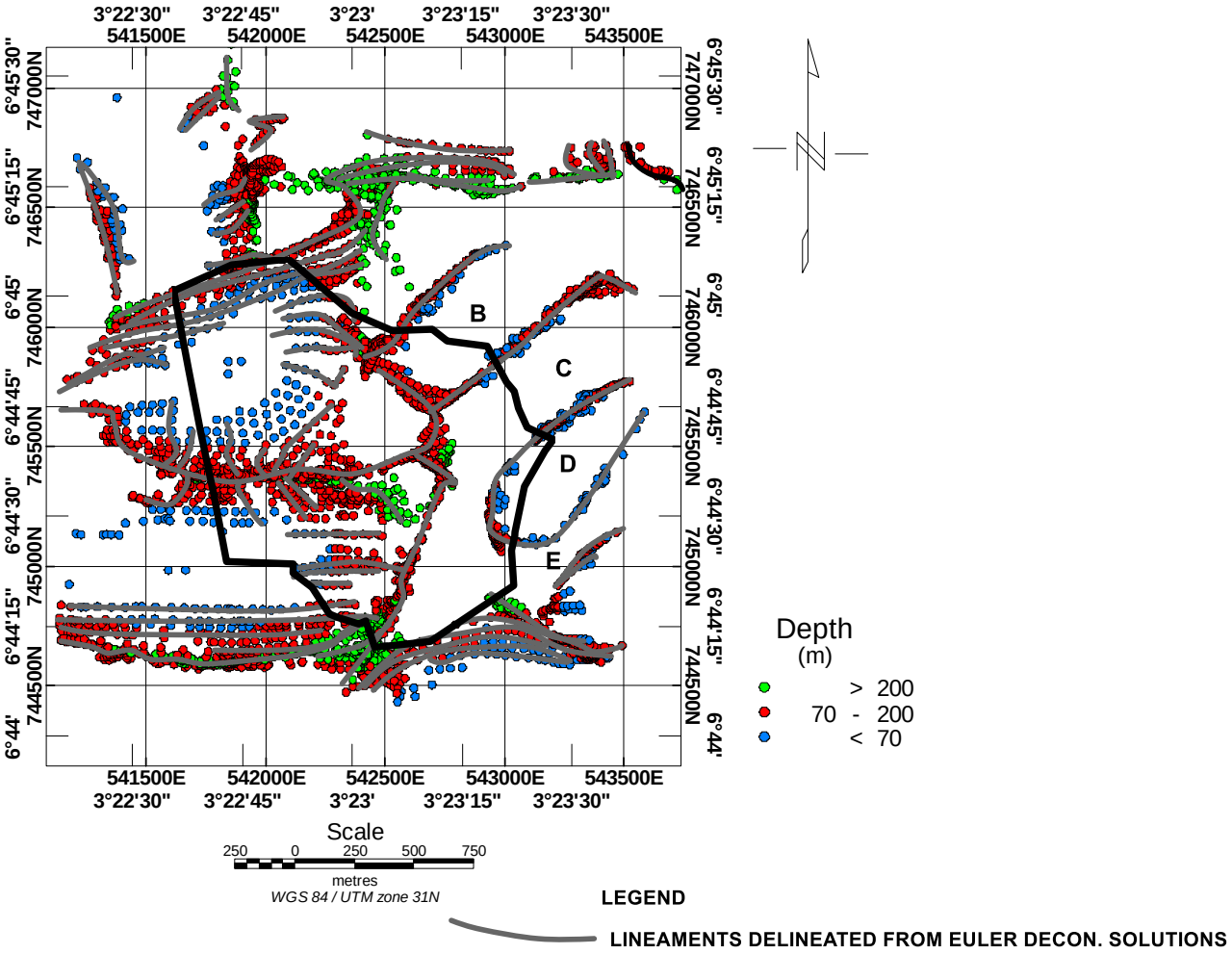

Figure 4.6(a): The Euler Deconvolution Solution Plot of the Study Area

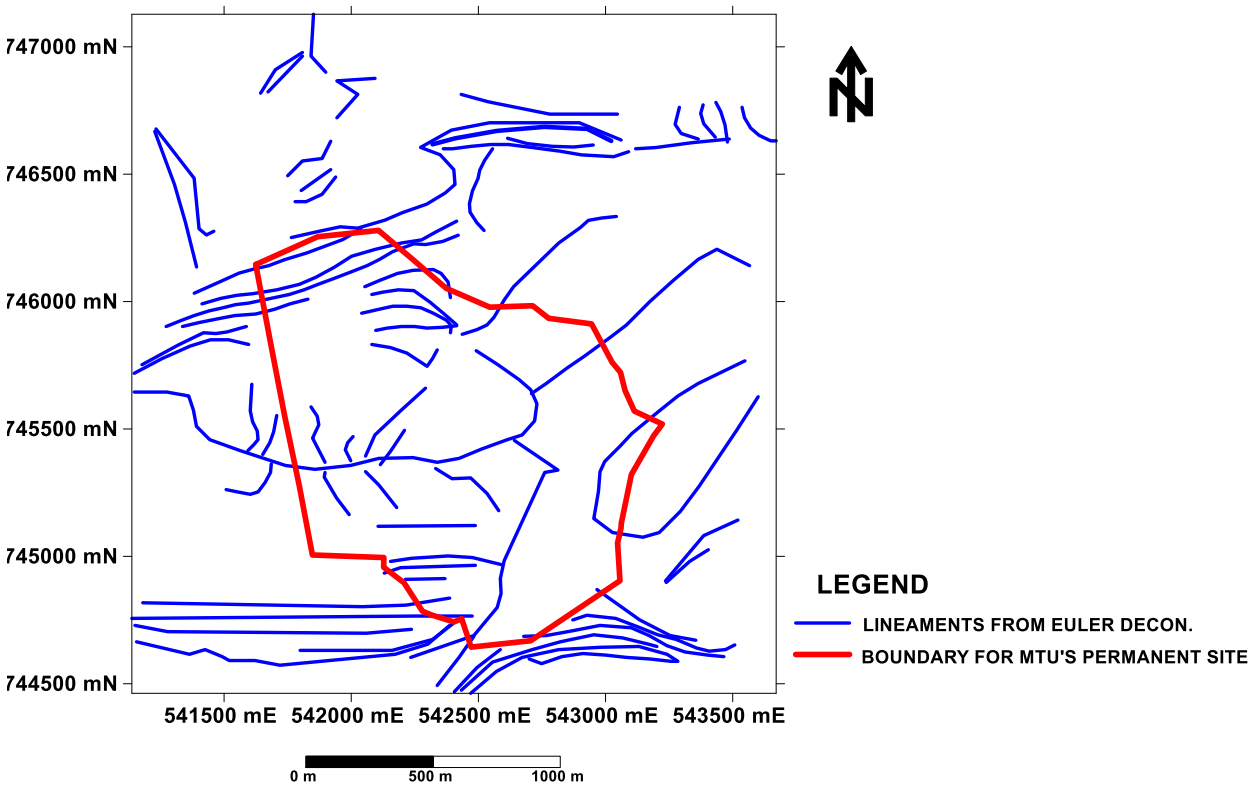

Figure 4.6(b): The Lineaments Delineated from Total Euler Deconvolution Solution Plot

4.2.3 Tilt Derivative (TDR)

In the interpretation of tilt derivative solutions (map), 0^o lines are taken to represent regions of discontinuities (lineaments). The tilt derivative solutions delineated three major lineaments (Figure 4.7 (a) and (b)). The lineaments delineated by tilt derivative are regional in nature and it sufficiently outlined the edges of the intersecting magnetic lows designated "Y" on the residual field map presented in Figure 4.3. The "Y" region are presented as a zone of weakness.`

4.2.4 Integration of the Extracted Lineaments from the aeromagnetic data using the Various Enhancement Techniques

The lineaments delineated by the THD comprised of long, intermediate and short lineaments. The western and southern parts consist mostly of long and intermediate lineaments while the northeastern part is dominated by short lineaments (Figure 4.5(b)). The Euler Deconvolution mostly resolved long lineaments and their appendages but resolved less of isolated short lineaments (Figure 4.6(b)). The integrated result of the THD and Euler deconvolution derived lineaments appreared to be confirmatory in most parts (i.e. the results agreed) while in some parts it was complementary as they seemed to complement each other (Figure 4.8(a)).

In order to reduce overclustering of the lineaments as was observed in Figure 4.8(a), lineaments greater than 200 m for the THD, Euler deconvolution and TDR were presented in Figure 4.8(b). The lineaments have orientations ranging from N-S, E-W, NW-SE and NE-SW though the dominant orientations are the E-W and the NW-SE orientations (Figure 4.9). The fault line seen on the geologic map presented in Figure 1.3 was observed to fall within a delineated zone of weakness.

4.2.5 Comparison of Depth Estimates from Euler Deconvolution and Tilt Derivative

Based on the Euler deconvolution map, the depth of lineaments delineated rarely exceeded 200 m except in the central southern and central northern parts where parts of a few lineament were found to be deeper (Figure 4.6(a)). To estimate depths to delineated lineaments (usually located on 0^o

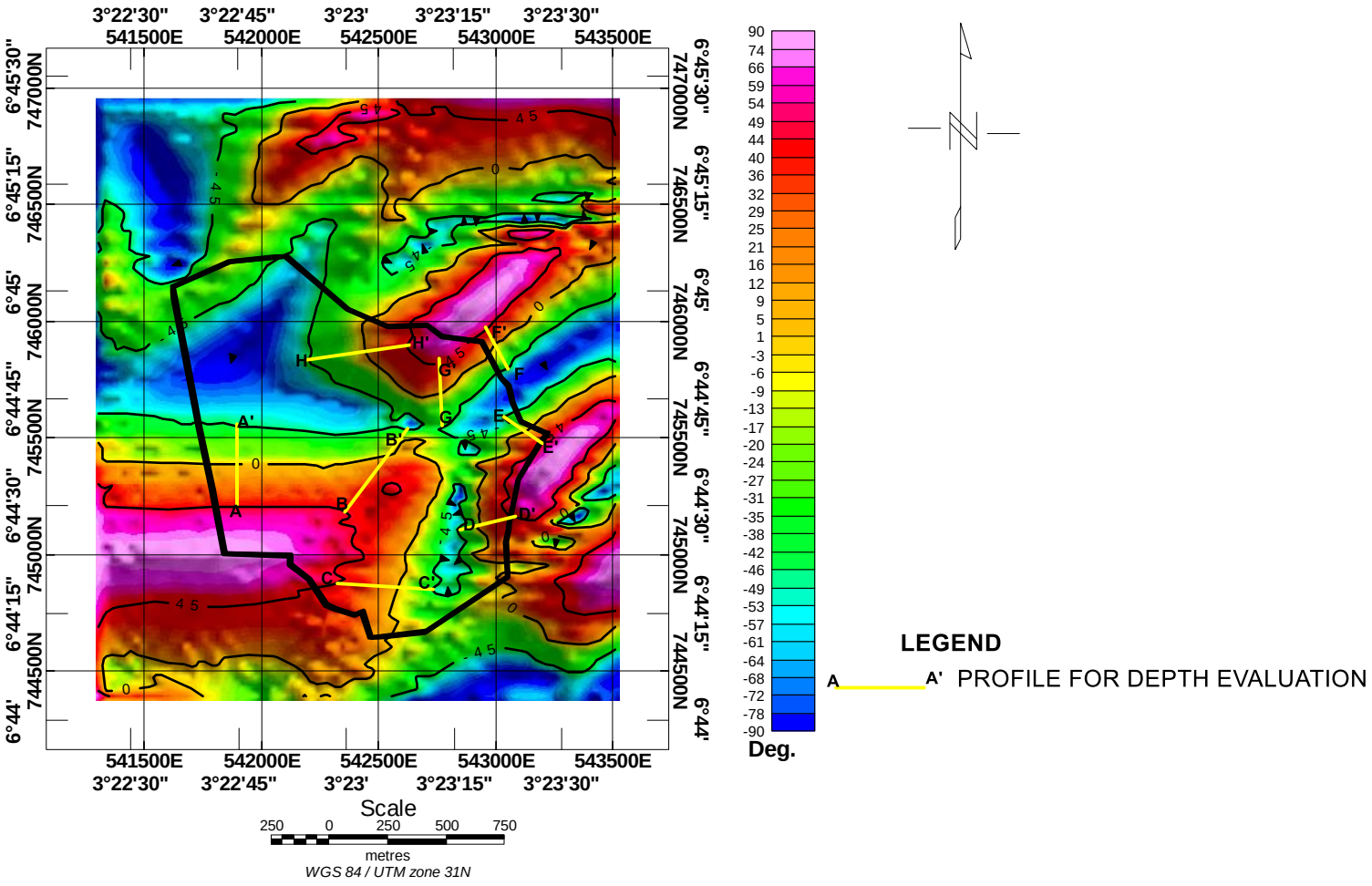

Figure 4.7(a): The Tilt Derivative Map of the Study Area

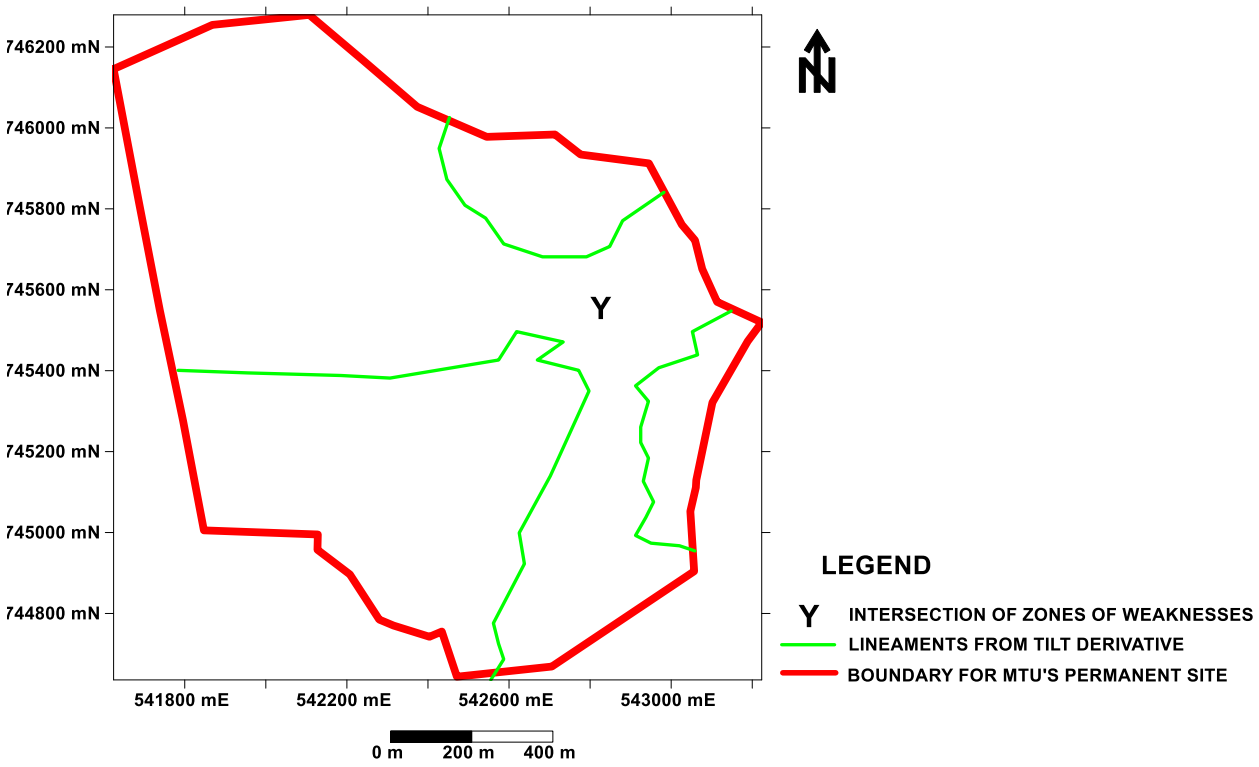

Figure 4.7(b): The Lineaments Derived from the Tilt Derivative Map of the Study Area

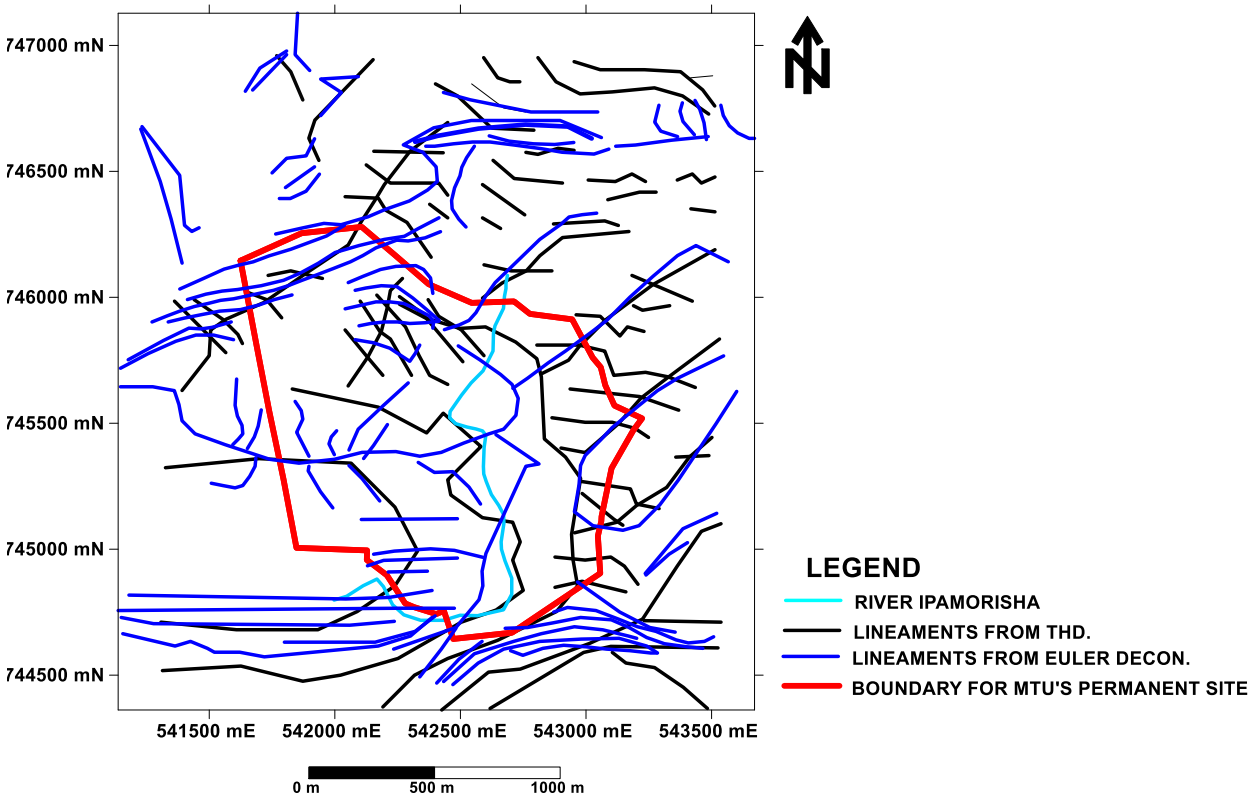

Figure 4.8(a): Integrated Lineaments Derived from the THD and Euler Deconvolution Operations

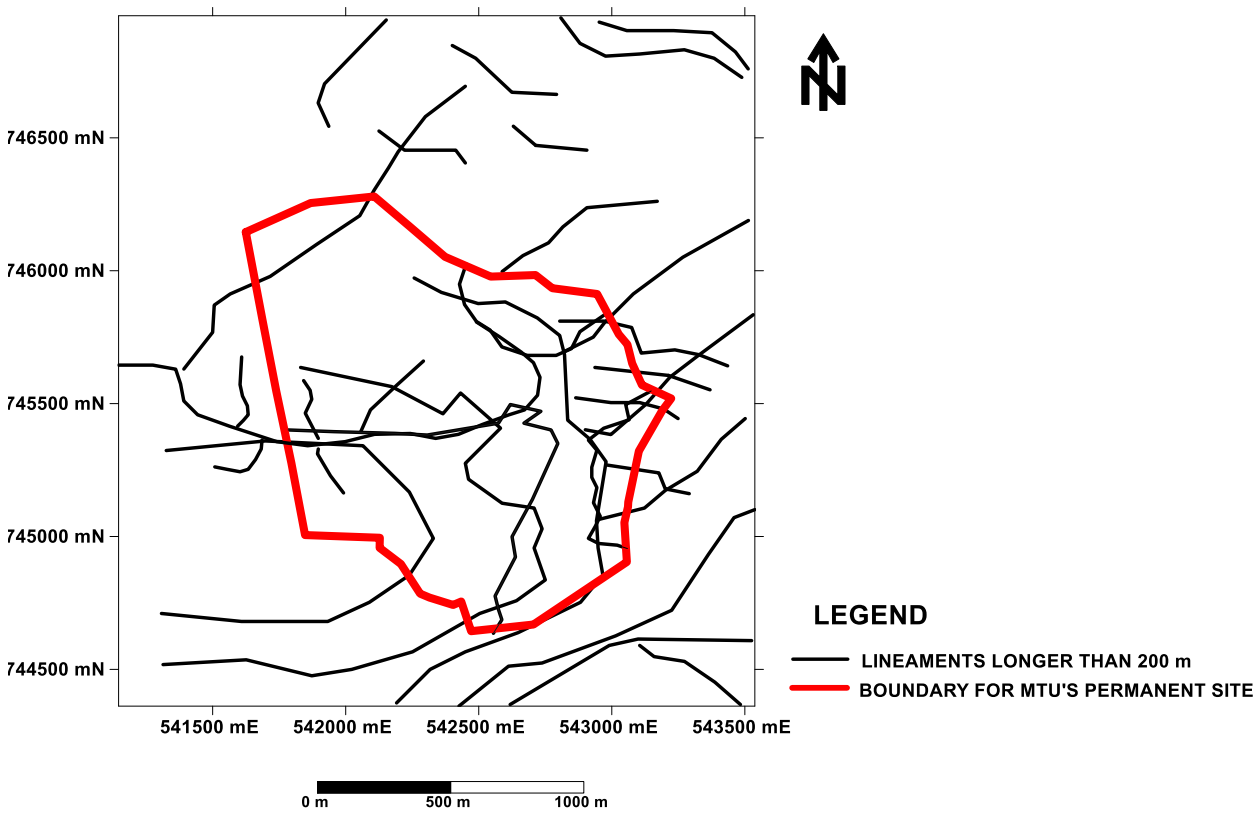

Figure 4.8(b): Lineaments Longer than 200 m Derived from the Combination of THD, Euler Deconvolution and Tilt Derivative Operations

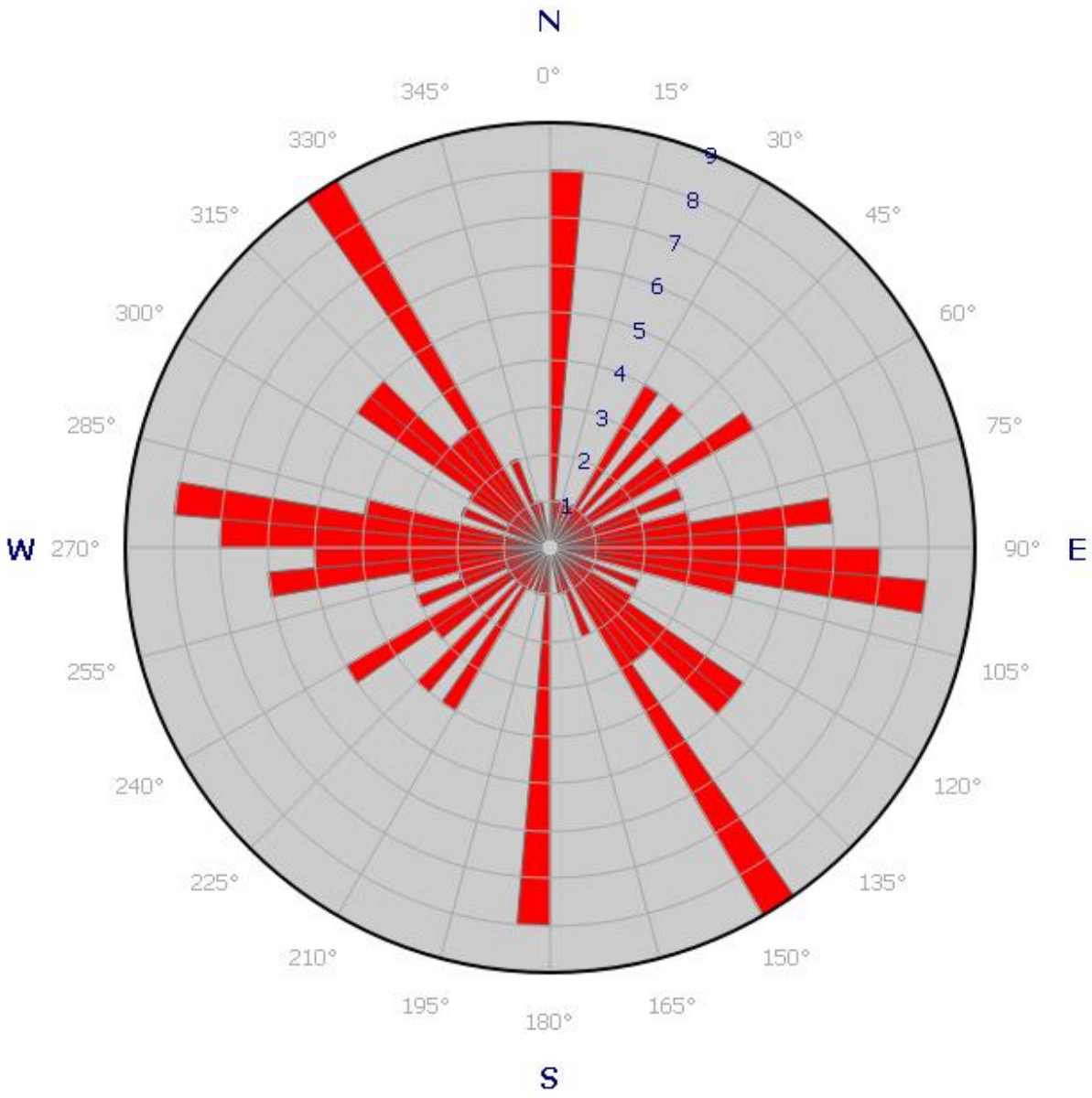

Figure 4.9: Rose Diagram Showing the Orientations of the Magnetic Lineaments Delineated.

contour lines) on the tilt derivative map, distance between +45^{o} and -45^{o} contour lines are determined and depth to the 0^{o} contour line (indicating locations of linear geologic structures) located between the +45^{o} and -45^{o} contour lines, are computed as half the distance obtained between +45^{o} and -45^{o} contour lines, using the scale of the map.

To determine depths to the southwestern structure on the tilt derivative map, Profiles A-A', B-B' and C-C' were taken over the structure and the depths obtained were 176.44 m, 235.29 m and 286.76 m respectively. To determine depths to the eastern structure, Profiles D-D' and E-E' were taken over it and the depths obtained were 132.35 m and 110.29 m respectively. To determine the depths to the northeastern structure, Profiles F-F', G-G' and H-H' were taken over it and the depths obtained were 102.94 m, 147.06 m and 220.59 m respectively.

Intepreted in terms of dip, the northeastern structure dips towards the west within the study area, while the southwestern and eastern stuctures both dip towards the south.

4.3 The 2D Electrical Resisitivity Tomography (ERT) Data Interpretation

Four 2D ERT data, labelled 2D ERT Line 1, 2D ERT Line 2, 2D ERT Line 3 and 2D ERT Line 5, were acquired within the study area. The four profiles were 1110 m long and probed up to a depth of 220 m. When superimposed on the delineated magnetic lineaments (Figure 4.10), the 2D ERT profiles were found to cut across some of the lineaments.

4.3.1 2D ERT Line 1 (Figure 4.11(a))

As observed on Figure 4.10, "2D ERT Line 1" was noted to cut across 7 magnetic lineaments which are located at 117 m, 208 m, 243 m, 299 m, 425 m, 741 m and 891 m from the start of profile. Only the lineaments located at 117 m (110 m on 2D ERT profile), 208 m to 243 m (200 to 250 m on 2D ERT profile), 425 m (440 m on 2D ERT profile) and 891 m from the start of profile were visble on the 2D ERT section. Point 741 from the start of line only showed as a "kink", designated as K, on the 2D ERT section (Figure 4.11(a)). To a good approximation, three basic

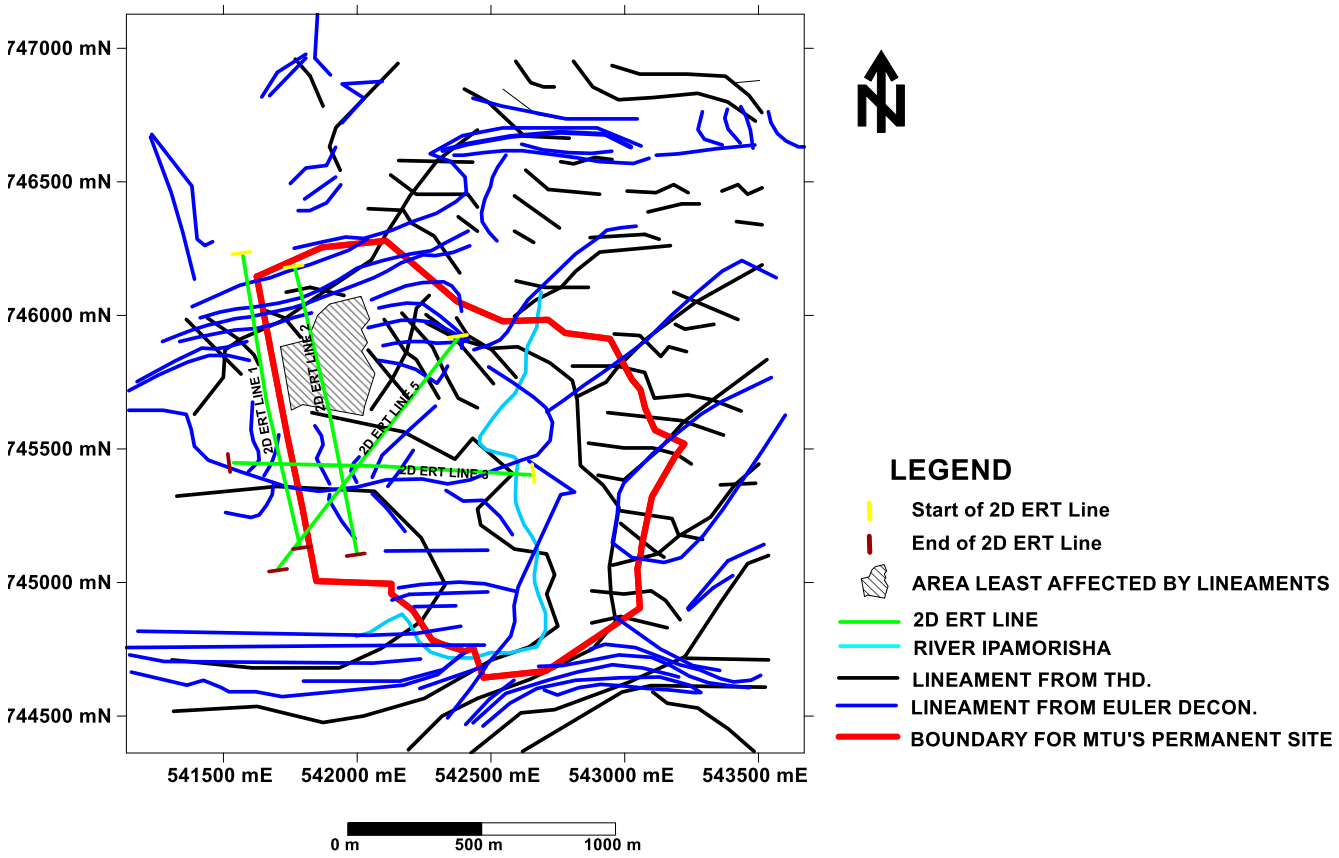

Figure 4.10: Map Showing the Positions of the 2D ERT Profiles Relative to the Delineated Magnetic Lineaments

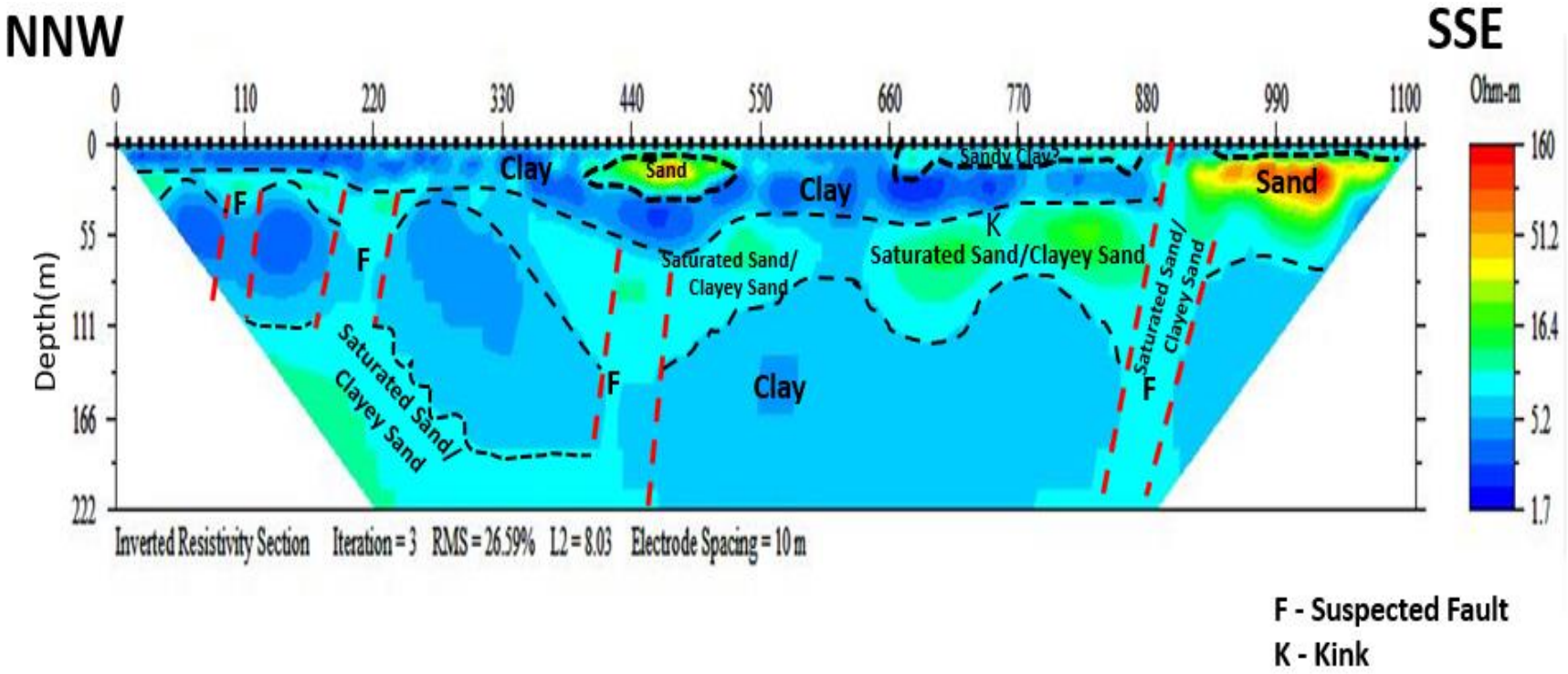

Figure 4.11(a): 2D ERT Line 1

lithologies (which are clay, sand and saturated sand/clayey sand) constituting four geoelectric/geologic layers which include a “clay” first layer, a “saturated sand/clayey-sand” second layer, a “clay” third layer and a “saturated sand/clayey sand” fourth layer were delineated in the northern section. In the central part (400 m to 530 m), a pocket of sand was delineated to be embeded within the first layer which is clay. At the southern end, three geoelectric layers which include a topmost thin layer of clay, followed by a considerably thick layer of sand (about 70 m) extending from a depth of about 8 m to 77.5 m, and last layer which is clayey in nature.

4.3.2 2D ERT Line 2 (Figure 4.11(b))

This profile is located 230 m east of “2D ERT Line 1”. As can be seen on Figure 4.10, “2D ERT Line 2” cuts across 8 magnetic lineaments which were located at 22 m, 99 m, 131 m, 161 m, 196 m, 589 m, 870 m and 1050 m from the start of profile. At about 195 to 225 m from the start of the profile is a region between two kinks, K_1 and K_2, conciding with the begining of a conspicous fault region which has been filled with sand (Figure 4.11(b)). K_1 is suspected to be the magnetic lineament intersected by the 2D ERT at 196 m from the start of profile. Points 870 to 890 m and 940 m to 990 m away from the start of the profile also appeared on the 2D ERT as “fault regions” and this also agreed in part with the result of the magnetic method that delineated a lineament at 870 m from the start of 2D ERT Line 2. The magnetic data seemed to be very responsive to edges formed by deposited superficial aggregate of earth materials (sand) as some magnetic lineaments (131 m , 161 m, 589 m and 1050 m) were found to be coincident with edges of gentle to signifcantly undulating layer of sand (undulating thickness of sand strata). A suspected ancient river channel was imaged at point 410 m from the start of line on the 2D ERT section. Just as was observed along profile 2D ERT Line 2, three basic lithologies which were “clay”, “sand” and “saturated sand/clayey-sand” were delineated.

4.3.3 2D ERT Line 3 (Figure 4.11(c))

As observed on Figure 4.10, “2D ERT Line 3” was noted to cut across 7 magnetic lineaments which were located at 82 m, 170 m, 494 m, 681 m, 802 m, 981 m and 1037 m from the start of

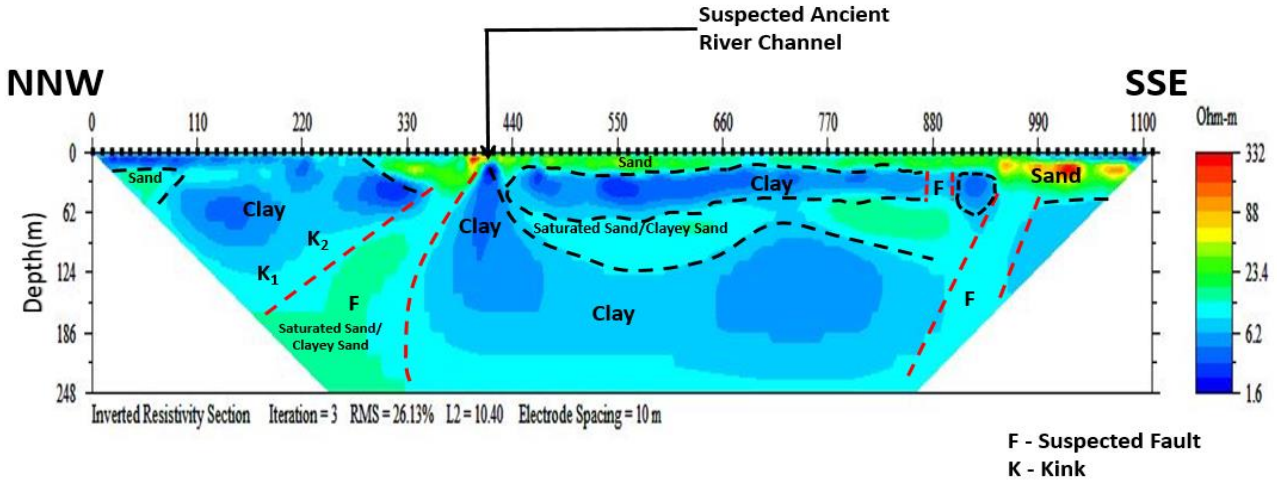

Figure 4.11(b): 2D ERT Line 2

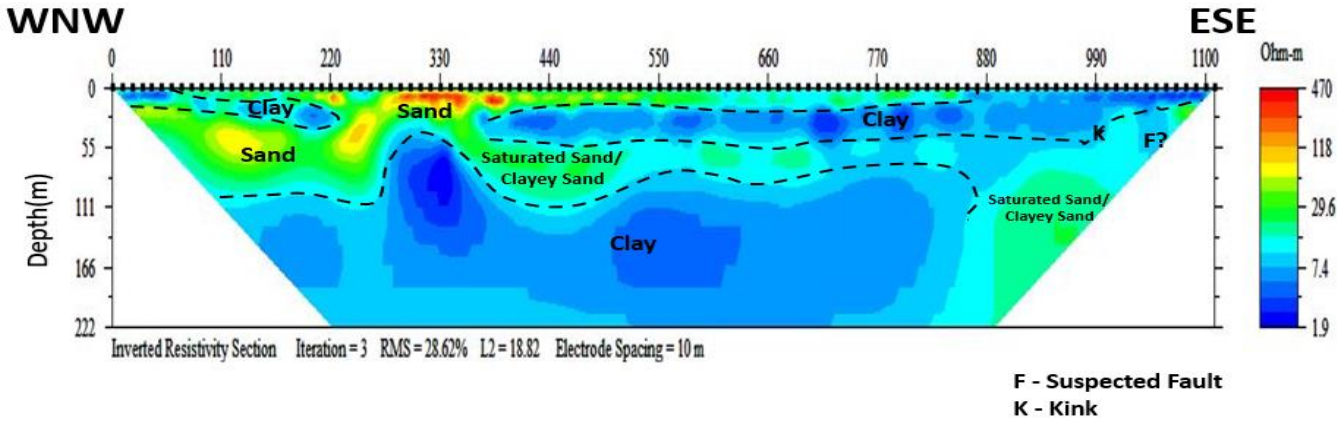

Figure 4.11(c): 2D ERT Line 3

profile. Only the magnetic lineaments located at 981 m and 1037 m from the start of the 2D ERT Profile (2D ERT Profile 3), were consipicously imaged on the 2D ERT section. The lineament located at 981 m from the start of line was imaged as a prominent edge (labelled K on the ERT section) on a sand deposit at the eastern end and the lineament located at 1037 m from the start of the profile concides with a depression (labelled F?) on the ERT section. The lithologies delineated here were basically sand and clay.

4.3.4 2D ERT Line 5 (Figure 4.11(d))

As observed on Figure 4.10, "2D ERT Line 5" is a NE-SW trending profile cuting across 7 magnetic lineaments which are located at 0 m, 26 m, 118 m, 192 m, 437 m, 656 m and 787 m from the start of profile. Points 192 m, 437 m and 656 m (610 – 640 m on the 2D ERT section) concide with suspected fault zones. Lithologies delineated are basically intercallation of sand and clay.

4.4 Implications of the Findings on the Physical Development of Mountain Top University's Permanent Site

Interpretation of the residual field and the lineament maps showed that the study area (Mountain Top University's permanent site) is a shear zone littered with lots of lineaments (Figures 4.3, 4.8(a) and 4.8(b)). The lineaments delineated have varying lengths. Depths of delineated lineaments rarely exceeded 287 m. In terms of lineament density, the least affected portion is a portion in the northwestern region identified as "area least affected by lineaments" (Figure 4.10). The implication of this is that the property must be developed with caution. The lineaments must be studied to determine if they are active or not before any form of construction. Special foundations may be required for construction. If faulted regions can be effectively stabilised for engineering constructions, the identified least affected portion by lineaments can then be used for landfill construction/waste management.

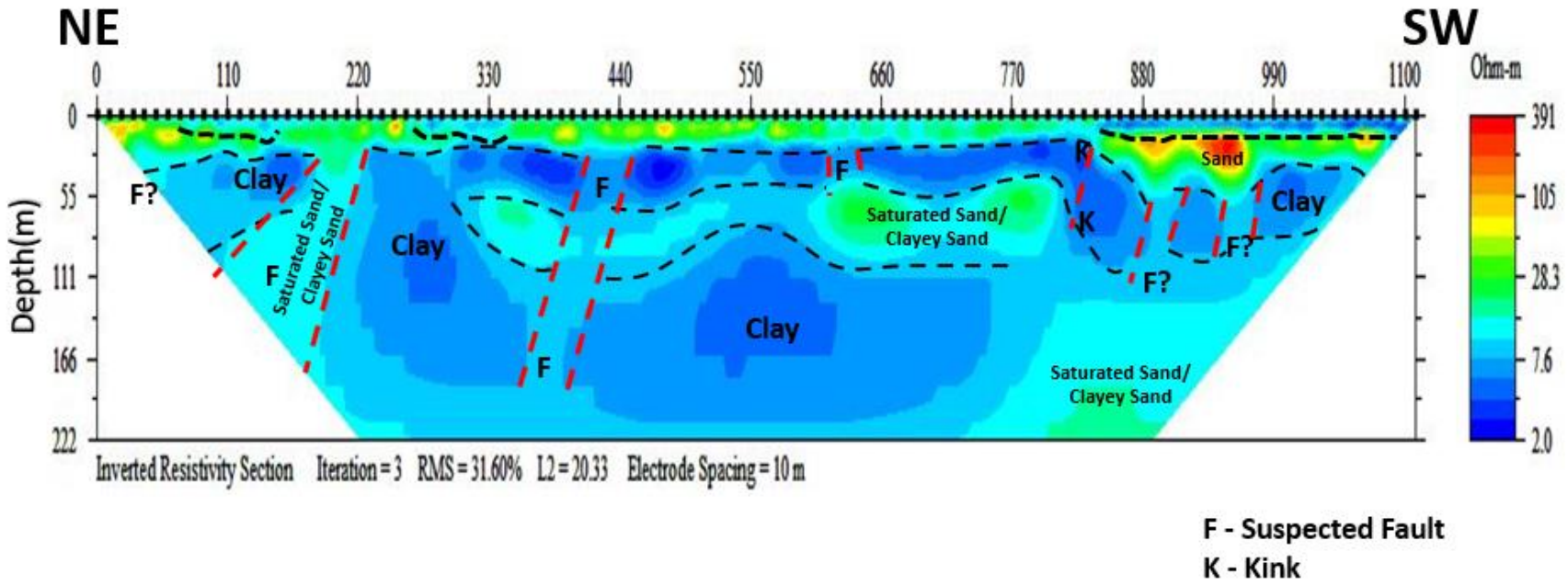

Figure 4.11(d): 2D ERT Line 5

As observed from the 2D ERT sections, the immediate topsoil at a considerable part of the study area is clay or clayey with thickness approching 8 m in some areas (e.g. northern to central part of 2D ERT Line 1, northern end of 2D ERT Line 2, eastern end of 2D ERT Line 3 and southwestern end of 2D ERT Line 5). This implies that the subgrade soil may be plastic and incompetent to carry heavy engineering structures. Other than stabilisng the faults if found to be inactive, it is also necessary to restrict constructions to regions where the subgrade soil is sandy and have appreciable thickness (exceeding 5 m). Search for groundwater may be concentrated around mapped faults, especially the ones identified on the 2D ERT sections. Based on their appearance and resistivity values on the 2D ERT sections, the delineated faults are suspected to be filled with sand.

CHAPTER FIVE

SUMMARY, CONCLUSION AND RECOMMENDATION

5.1 Summary

Aeromagnetic and 2D electrical resistivity tomography data have been processed and interpreted for the purpose of delineating linear geologic structures present at Mountain Top University's permanent site in Makogi-Oba, Ibafo area of Ogun state with the aim of generating a lineament map showing the density, orientation and approximate depths of occurrence of the linear structures which would guide developmental planning within the area.

The TMI map was observed to be dominated by elongated to linear magnetic anomalies trending mostly in the approximate N – S direction. Though having a low magnetic relief of about 2.6 nT, the study area reflected four magnetic field intensity zones which are characteristically distinct with magnetic intensity decreasing from West to East. The pattern of the decreasing magnetic intensities eastwards seems to be suggestive of a step-faulting phenomenon with depth to the faulted blocks decreasing eastwards.

The residual field map was observered to comprise both elongated and spherical magnetic anomalies, some with relatively high magnetic intensities while some have relative low magnetic intensities. A comparison of the TMI and residual field maps showed that the residual map accentuated the short wavelength structures and suppressed the long wavelength structures that dominated the TMI map significantly. An intersection of magnetic lows in the eastern part of the study area was identified and interpreted to suggest that the study area is a shear zone.

Lineament enhancement techniques applied include the Total Horizontal Derivative (THD), Euler Deconvolution and the Tilt Derivative. The lineaments delineated by the THD comprised of long,

intermediate and short lineaments. From the THD map, the western and southern parts consist mostly of long and intermediate lineaments while the northeastern part is dominated by short lineaments. The Euler Deconvolution mostly resolved long lineaments and their appendages but resolved less of isolated short lineaments. The integrated result of the THD and Euler deconvolution derived lineaments appreared to agree in a good part of the study area while in some parts it can be best described as complementary as the lineaments from both THD and Euler Deconvolution seemed to complement each other. The tilt derivative solutions delineated three major lineaments which are regional in nature. It sufficiently outlined the edges of the intersecting magnetic lows designated "Y" on the residual field map such that region "Y" was delineated as a zone of stuctural weakness.`

The Euler Deconvolution solutions showed that depth estimates of linear geologic structures rarely exceed 200 m in the study area except in the central southern and central northern parts. Tilt derivative solutions present depth to some delineated semi-regional to regional scaled structures to range between 102.94 m and 286.76 m.

Four 2D ERT data with a spread of 1110 m, cutting across delineated magnetic lineaments and probing a depth of 220 m were acquired. Some of the delineated magnetic lineament were confiremed on the 2D ERT sections to be genuine geologic faults while others only corresponded to edges along delineated strata of sand layer. The lithologies delineated were basically sand and clay.

5.2 Conclusion

The study area was found to be a shear zone having lots of linear geologic structures within it. At least three tectonic events were established based on their imprints. The oldest was a first NE-SW trending event, the second was the approximate NW-SE event and the last observable event was another NE-SW trending event which appeared to be the youngest of all the events.

With respect to developmental planning, since lineament density seems to be high, the study area must be developed with caution. The lineaments must be studied to determine if they are active or not before any form of construction. The immediate topsoil at a good part of the study area is clay with thickness approaching 8 m in some areas. This implies that the subgrade soil may be plastic and incompetent to carry heavy engineering structures. Other than stabilisng the faults if found to be inactive, it is also necessary to restrict constructions to regions where the subgrade soil is sandy and have appreciable thickness (exceeding 5 m).

Groundwater exploration should be concentrated around mapped faults, especially the ones identified on the 2D ERT sections.

5.3 Recommendation

Since lineament density is high within the study area, it has to be determined if the fault zones are active. If not active, construction can be done within the area but it should be ensured that buildings are not built to straddle fault zones and adjacent regions with no fault as this will encourage differential settlement. Required engineering reinforcement should be put in place to hold buildings in place when planning to build in this region. In order to optimize the groundwater resources in the area, the linear geologic structures should be intersected at the region where they dip towards.

REFERENCE

Abdullah, A., Nassr, S., and Ghaleeb, A. (2013). Remote Sensing and Geographic Information System for Fault Segments Mapping a Study from Taiz Area, Yemen. Journal of Geological Research.

Adagunodo, T.A., Sunmonu, L.A. and Adetunji, A.A. (2015). An Overview of Magnetic Method in Mineral Exploration. Journal of Ecology and Environment 3(1), pp. 13-28

Adamo, N., Al-Ansari, N., Sissakian, V., Laue, J. and Knutsson, S. (2021). Geophysical Methods and their Applications in Dam Safety Monitoring. Journal of Earth Sciences and Geotechnical Engineering, 11(1), 291-345.

Adeleke, B. O. and Leong, G. C. (1978). Certificate Physical and Human Geography, West African Ed. Oxford University Press, Nigeria, Ibadan. pp. 32.

Adewumi, I., and Olorunfemi, M. O. (2005). Using geoinformatics in construction management. Journal of Applied Sciences(Pakistan), 5(4), 761-767.

Aina, A., Olorunfemi, M. O. and Ojo, J. S. (1996). An integration of aeromagnetic and electrical resistivity methods in dam site investigation. Geophysics, 61(2), 349-356.

Amadi, A. N., Eze, C. J., Igwe, C. O., Okunlola, I. A., and Okoye, N. O. (2012). Architect's and Geologist's View on the Causes of Building Failures in Nigeria. Modern Applied Science, 6(6), 31.

Arora, K., Cazenave, A., Engdahl, E. R., Kind, R., Manglik, A., Roy, S., and Uyeda, S. (2011). Encyclopedia of solid earth geophysics. Springer Science & Business Media.

Balogun, O. B. (2019). Tectonic and structural analysis of the Migmatite–Gneiss–Quartzite complex of Ilorin area from aeromagnetic data. NRIAG Journal of Astronomy and geophysics, 8(1), 22-33.

Balogun, O.B, Ojo, S.B and Olorunfemi, M.O (2016). Characterisation of the tectonic lineaments in the central equatorial Atlantic region of Africa from Bouger anomaly gravity data. Ife Journal of Science 18(4); 931-947.

Blakely, R. J. (1996). Potential theory in gravity and magnetic applications. Cambridge university press.

Bogoslovsky, V. A., and Ogilvy, A. A. (1977). Geophysical methods for the investigation of landslides. Geophysics, 42(3), 562-571.

Cardarelli, E., Cercato, M., Cerreto, A. and Di Filippo, G., 2010. Electrical resistivity and seismic refraction tomography to detect buried cavities. *Geophysical prospecting*, *58*(4), pp.685-695.

Chirindja, F. J., Dahlin, T. and Juizo, D. (2017). Improving the groundwater-well siting approach in consolidated rock in Nampula Province, Mozambique. *Hydrogeology Journal*, 25(5), 1423-1435.

Curtis, C. and Low, N. (2016). Institutional barriers to sustainable transport. Routledge, pp.

Davis, K., Li, Y. and Batzle, M. (2008). Time-lapse gravity monitoring: A systematic 4D approach with application to aquifer storage and recovery. Geophysics, 73(6), WA61-WA69.

De Klasz, I., and Du Chêne, R. J. (1978). Presence of Albian-Cenomanian in southwestern Nigeria and its paleogeographic implications. Compte Rendu de la Société de Physique et d'Histoire Naturelle de Genève, 13, 10-15.

Dearman, W. R. (2013). Engineering geological mapping. Elsevier.

Delury, D.B (1950). Values and Integrals of the orthogonal polinomials up to n = 26. University of Toronto press.

Ejepu, J. S., Olasehinde, P., Okhimamhe, A. A., and Okunlola, I. (2017). Investigation of Geological Structures of Hydrogeological Importance of 1: 100,000 Sheet 185 (Paiko) North-Central Nigeria Using Integrated Geophysical and Remote Sensing Techniques.

Fairbridge, R.W., Askew, A.J., Herschy, R.W., Herschy, R.W., Herschy, R.W., Hordon, R.M., Muller, R.A., Grymes, J.M., Fairbridge, R.W., Herschy, R.W. and Brassington, F.C., 1998. Water movement in unsaturated soils. *Encyclopedia of Hydrology and Water Resources*, pp.699-706.

Fairhead, J. D., Salem, A., and Williams, S. E. (2009). PS Tilt-Depth: A Simple Depth-Estimation Method Using First Order Magnetic Derivatives.

Francisco J. F. Ferreira, Luís G. de Castro, Alessandra B. S. Bongiolo, Jeferson de Souza, and Marco A. T. Romeiro, (2011), "Enhancement of the total horizontal gradient of

magnetic anomalies using tilt derivatives: Part II — Application to real data," *SEG Technical Program Expanded Abstracts* : 887-891.

Google Maps (2020), Mountain Top University Permanent Site, Makogi-Oba, Ogun State, Nigeria, 1: 1500. Google Maps Online, Accessed August, 2021.

Gore, D. and Davies, P. (2013). Background paper on produced water and solids in relation to coal seam gas production.

Grant, F.S (1957). A problem in the analysis of geophysical data. Geophysics 22, 309-344.

Griffiths, D.H. and King, R.F., 2013. *Applied geophysics for geologists and engineers: the elements of geophysical prospecting, pp. 1-5*. Elsevier.

Holden, J., Burt, T.P and Vilas, M. (2002). Application of ground-penetrating radar to the identification of subsurface piping in blanket peat. *Earth Surface Processes and Landforms, 27*(3), pp.235-249

Hossain, M. S., Dharmateja, M., and Hossain, J. (2010). Assessment of geo-hazard potential and site investigations using Resistivity Imaging. International Journal of Environmental Technology and Management, 13(2), 116-129.

Isaksson, H., Thunehed, H., Pitkänen, T., and Keisu, M. (2007). Forsmark site investigation. Detailed ground magnetic survey and lineament interpretation in the Forsmark area, 2006-2007 (No. SKB-R--07-62). Swedish Nuclear Fuel and Waste Management Co.

Kearey, P., Brooks, M., and Hill, I. (2002). An introduction to geophysical exploration. John Wiley and Sons.

Lowe, J. and Zaccheo, P.F., 1991. Subsurface explorations and sampling. In *Foundation Engineering Handbook* (pp. 1-71). Springer, Boston, MA.

Lowrie, W. (2007). Seismic wave propagation. In Lowrie W. (2nd Ed). Fundamentals of Geophysics. Cambridge University Press, pp. 171-192,

Mattsson, H., and Wahlgren, C. H. (2010). Interpretation of detailed ground magnetic data, resistivity and topographic data from Äspö (No. SKB-P--10-49). Swedish Nuclear Fuel and Waste Management Co.

McDowell, P.W., Barker, R.D., Butcher, A.P., Culshaw, M.G., Jackson, P.D., McCann, D.M., Skipp, B.O., Matthews, S.L. and Arthur, J.C.R. (2002). *Geophysics in engineering investigations* (Vol. 19). London: Ciria.

Momoh, J. A., Xia, Y., and Boswell, G. D. (2008, September). An approach to determine Distributed Generation (DG) benefits in power networks. In 2008 40th North American Power Symposium (pp. 1-7). IEEE.

National Research Council. (2004). Groundwater fluxes across interfaces. National Academies Press

Okpoli, C. C., and Oludeyi, D. (2019). Aeromagnetic Mapping of Iwo Region of Southwestern Nigeria for Lithostructural Delineation. Pakistan Journal of Geology, 3(2), 20-30.

Okunubi and Olorunfemi (2016). Integrated geophysical investigation of remotely sensed suspected fault zones around Iwaraja-Ijebu Ijesa area of Osun state, Nigeria. *Ife Journal of Science*, *18*(1), pp.133-145.

Oladejo, O. P., Adagunodo, T. A., Sunmonu, L. A., Adabanija, M. A., Enemuwe, C. A., and Isibor, P. O. (2020). Aeromagnetic mapping of fault architecture along Lagos–Ore axis, southwestern Nigeria. Open Geosciences, 12(1), 376-389.

Oladele, S., and Ayolabi, E. A. (2014). Geopotential imaging of the benin basin for hydrocarbon prospectivity. NAPE Bull, 26(1), 101-112.

Oldham, C.H.G and Sutherland, D.B. (1955). Orthogonal polynomials, their used in the estimating the regional effect. Geophysics **20**, 295-306

Olorunfemi, M. O. and Oni, A. G. (2019). Integrated geophysical methods and techniques for siting productive boreholes in basement complex terrain of southwestern Nigeria. *Ife Journal of Science*, 21(1), 13-26.

Olorunfemi, M. O., Oni, A. G., Bamidele, O. E., Fadare, T. K. and Aniko, O. O. (2020). Combined geophysical investigations of the characteristics of a regional fault zone for groundwater development in a basement complex terrain of South-west Nigeria. *SN Applied Sciences*, 2(6), 1-17.

Olorunfemi, M. O., Oni, A. G., Fadare, T. K. and Bamidele, O. E. (2021). Linear geological structure, traverse orientation and structure resolution and characterisation using 1D and 2D resistivity images. *NRIAG Journal of Astronomy and Geophysics*, 10(1), 170-184.

Omatsola, M. E. (1981). Tectonic evolution and Cretaceous stratigraphy of the Dahomey Basin. J. Min. Geol., 18, 130-137.

O'Neill, M. W. (2001). Side resistance in piles and drilled shafts. *Journal of Geotechnical and Geoenvironmental Engineering*, 127(1), 3-16.

Oni, A. G., Adediran, T. A., Olorunfemi, M. O., Eniola, P. J., and Adewale, E. A. (2020). Evaluation of the groundwater potential of Modomo Community in Ile-Ife, Southwest Nigeria, using integrated geophysical techniques. Sustainable Water Resources Management, 6(6), 1-18.

Oyedele, K. F., and Olorode, D. O. (2010). Site investigations of subsurface conditions using electrical resistivity method and cone penetration test at Medina Estate, Gbagada, Lagos, Nigeria.

Oyeniyi, T. O., Salami, A. A., and Ojo, S. B. (2016). Magnetic surveying as an aid to geological mapping: a case study from Obafemi Awolowo university campus in Ile-Ife, southwest Nigeria. Ife Journal of Science, 18(2), 331-343.

Ozegin, K. O., Oseghale, A. O., Audu, A. L. and Ofotokun, E. J. (2013). An application of the 2D DC Resistivity method in Building Site Investigation–a case study: South-South Nigeria. *Journal of Environment and Earth Science*, 3(2), 108-112.

Parsekian, A. D., Singha, K., Minsley, B. J., Holbrook, W. S. and Slater, L. (2015). Multiscale geophysical imaging of the critical zone. Reviews of Geophysics, 53(1), 1-26.

Paterson, N. R., and Reeves, C. V. (1985). Applications of gravity and magnetic surveys: The state-of-the-art in 1985. Geophysics, 50(12), 2558-2594.

Rana, S. (2019). Geophysical Investigations to Deal with Uncertainties in Difficult Ground Conditions. ISRM India Journal-Half Yearly Technical Journal of Indian National Group of ISRM, 8(2), 25-30.

Reid, A. B., Allsop, J. M., Granser, H., Millett, A. T., and Somerton, I. W. (1990). Magnetic interpretation in three dimensions using Euler deconvolution. Geophysics, 55(1), 80-91.

Reynolds, J. M. (1997): An Introduction to Applied and Environmental Geophysics 1997 John Wiley and Sons Ltd. New York.

Reynolds, J. M. (2011). An introduction to applied and environmental geophysics. John Wiley & Sons.

Ribes, D. and Finholt, T. A. (2009). The long now of infrastructure: Articulating tensions in development. Paul Edwards, Geoffrey C. Bowker, Steven Jackson, and Robin Williams (Eds). Volume 10, Special Issue 5, pp. 375-398.

Robinson, D. A., Binley, A., Crook, N., Day-Lewis, F. D., Ferré, T. P. A., Grauch, V. J. S., and Slater, L. (2008). Advancing process-based watershed hydrological research using near-surface geophysics: A vision for, and review of, electrical and magnetic geophysical methods. Hydrological Processes: An International Journal, 22(18), 3604-3635.

Salem, A., Williams, S., Fairhead, J. D., Ravat, D. and Smith, R. (2007). Tilt-depth method: A simple depth estimation method using first-order magnetic derivatives. The leading edge, 26(12), 1502-1505.

Telford, W. M., Telford, W. M., Geldart, L. P., and Sheriff, R. E. (1990). Applied geophysics. Cambridge university press.

Udensi, E. E., and Osazuwa, I. B. (2004). Spectral determination of depths to magnetic rocks under the Nupe Basin, Nigeria. Nigerian Association of Petroleum Explorationists Bulletin, 17, 227.

USGS (2006) Shuttle radar topography mission, 1 Arc second scene, filled-finished-B, global land cover facility, Maryland: University of Maryland, College Park.

Verduzco, B., Fairhead, J. D., Green, C. M., and MacKenzie, C. (2004). New insights into magnetic derivatives for structural mapping. The leading edge, 23(2), 116-119.

Walters, K.A. (2008). Investigation of construction practices and test procedures for road pavements on expansive subgrades, pp. 1-331

Internet Resources

https://www.en.climate-data.org/africa/nigeria/lagos/lagos-552/ Retrieved on August, 2021.

https://www.lagosstate.gov.ng/about-lagos/ Retrieved on August, 2021.